Improvement of affinity and potency of a monoclonal antibody against *Shigella flexneri* 3a O-antigen via phage display and whole-cell in-solution panning

Nicholas L. Xerri[1], Sophia Pulido[1], Mateusz Kędzior[1], Paul Savarino[1], Torrey Williams[1], Robert M. Gallant[1], Robert W. Kaminski[2], Devin Sok[3], Hayden R. Schmidt[1*]

[1] IAVI Neutralizing Antibody Center, San Diego, California, USA

[2] Latham Biopharm Group, Cambridge, Massachusetts, USA

[3] Global Health Investment Corporation, New York, New York, USA

[*]Correspondance: hschmidt@iavi.org

Abstract:
As rates of antimicrobial resistance (AMR) among bacterial pathogens continue to rise, the discovery and development of novel classes of therapeutics that can serve as alternatives or adjuncts to traditional small-molecule antibiotics, such as monoclonal antibodies (mAbs), is a public health priority. Some of the most promising antigen targets for antibacterial mAbs are surface polysaccharides such as O-antigen (O-Ag), a component of the lipopolysaccharide found on the outer membrane of gram-negative bacteria. However, developing mAbs against bacterial surface polysaccharides with sufficient breadth and potency to be clinically viable is difficult in part because antibodies against polysaccharides are generally low affinity, and the challenging biochemistry of polysaccharides often precludes further affinity maturation of mAbs against these targets *in vitro*. Here, we use a phage display library and a whole-cell in-solution panning strategy to successfully improve the affinity of a mAb against *Shigella flexneri* 3a O-Ag *in vitro* without requiring the purification of the target antigen. We demonstrate that a single mutation can improve apparent affinity approximately 10-fold without detectably increasing polyreactivity, and increased affinity correlates with enhanced potency in antibacterial effector function and anti-virulence assays. In addition, the most potent variants also gained increased breadth, successfully coordinating complement deposition and complement-independent opsonophagocytosis against *S. flexneri* 3b, a serotype weakly recognized by the parent mAb. Altogether, this work represents an important first step towards expanding the antibody engineering toolkit for bacterial surface polysaccharides, which will aid the development of novel mAb therapeutics against AMR bacterial pathogens.

Introduction:
Antimicrobial resistance (AMR) among pathogenic bacteria is a rapidly growing threat that necessitates the development of novel therapeutics to supplement existing antibiotics(1). Monoclonal antibodies (mAbs) may be complementary to antibiotics because they can prevent and treat AMR infections by both recruiting effector cells to kill bacteria via Fc-mediated effector functions (i.e., complement-driven bactericidal activity or complement independent opsonophagocytosis), and by directly interfering with bacterial virulence(2). Some of the most promising antigens for antibacterial immunotherapies are

polysaccharides on the bacterial surface. Surface polysaccharides are well validated targets for approved bacterial vaccines (e.g., those against *Haemophilus influenzae* b, *Streptococcus pneumoniae*, *Neisseria meningitidis*, and *Salmonella typhi*) (3–7). This provides a strong rationale for developing anti-polysaccharide mAbs, and anti-polysaccharide mAbs against several bacterial species have been shown to be effective in preclinical animal models (8–17). However, to date, few of these mAbs against bacterial polysaccharides have been evaluated in clinical trials. Panobacumab, an IgM mAb against O-antigen (O-Ag) from serotype O11 *Pseudomonas aeruginosa* obtained promising results in a phase IIa trial among patients with pneumonia, though the effect size was modest and no control arm was present (18), so additional studies are required to fully assess clinical benefit. Gremubamab, a bispecific mAb targeting the exopolysaccharide PsI and the protein PcrV, has entered the clinic (19) and recently shown promise in treating *P. aeruginosa* infections in patients with bronchiectasis, though similarly, this was a proof-of-concept trial and more studies are required to ensure reproducible clinical efficacy (20).

One reason for the small number of both clinical trials and anti-polysaccharide mAb candidates in the pipeline is that discovering and engineering anti-polysaccharide mAbs that have sufficient breadth and potency to be clinically viable is challenging. Breadth for a given anti-polysaccharide mAb is often too narrow for clinical use because the chemical structures of most surface polysaccharides are highly variable (even within the same bacterial species (21). Bacterial strains of a given species are typically grouped into serotypes (often dozens or more) based on the specific chemical structure of key surface polysaccharides (such as the O-Ag, which is a component of gram-negative lipopolysaccharide), and antibody responses against these bacteria are usually serotype-specific (22,23). In addition to breadth, potency is another challenge for anti-polysaccharide mAbs since B cells targeting repetitive polysaccharide antigens undergo T cell independent responses that generate short-lived plasma antibody responses, which are predominately IgM with minimal somatic mutation and low affinity for the target antigen (24). While there are examples of high affinity anti-bacterial polysaccharide mAbs that have undergone extensive affinity maturation isolated from the peripheral blood mononuclear cells of convalescent donors (16), it is unclear how widespread this phenomenon is. In principle, additional high-potency mAbs against bacterial surface polysaccharides can be developed by engineering high-affinity variants of known anti-bacterial polysaccharide mAbs through *in vitro* affinity maturation. The chemical heterogeneity, inherent complexity of polysaccharide biochemistry, and the conformational flexibility of these polysaccharides (leading to a high entropic cost for binding for mAbs (25)) makes achieving *in vitro* affinity maturation of these mAbs is difficult using standard approaches.

To date, relatively few successful attempts at *in vitro* affinity maturation of anti-glycan mAbs have been reported (26–35). Most of these efforts have targeted glycans that are easier to purify and lack the variable, highly repetitive architecture of polysaccharides like O-Ag or capsular polysaccharide. To our knowledge, the only bacterial O-Ag or capsular polysaccharide for which successful *in vitro* affinity maturation has been reported is the O-Ag from *Salmonella* serogroup B. However, the impact that improving the affinity of

these mAbs had on antibacterial effector functions was not explored (32,33,36). As a result, the relationship between antibody binding affinity and the potency of specific effector functions is less well characterized for mAbs against bacterial polysaccharides than for those against mammalian glycans.

Here, we utilize a creative whole-cell in-solution phage display panning strategy, coupled with next-generation sequencing, to overcome these challenges and improve the affinity of a prototypical anti-O-Ag mAb specific for *Shigella flexneri* serotype 3a. We demonstrate that one to two mutations are sufficient to not only improve potency across effector functions against the target serotype, *S. flexneri* 3a, but to also expand breadth to serotype 3b. Importantly, a lack of polyreactivity against other bacterial strains or common polyreactivity reagents such as single stranded DNA (ssDNA) indicates that these improvements in binding are specific. Interestingly, binding affinity and potency are generally correlated for most effector functions, but are not necessarily interdependent, particularly for complement-independent opsonophagocytosis. Altogether, these data provide a framework for affinity maturing mAbs against bacterial polysaccharides *in vitro* and demonstrate that (at least in this test case) few mutations are needed to significantly improve the breadth and potency of an anti-O-Ag antibody.

Results:

hFlex3a2 functions as a chimeric huIgG1, but not as an scFv

hFlex3a2 is a murine hybridoma IgG3 that binds to *S. flexneri* 3a O-Ag and can coordinate complement-mediated bacteriolysis of this serotype in an antibody bactericidal assay (37). We determined the sequence of this mAb (Table S1) and found that it has many of the properties commonly associated with anti-O-Ag mAbs. The putative variable gene segment of the heavy chain of hFlex3a2 differs from the germline segment IGHV1-4*02, its closest germline progenitor, by only four amino acids, while the putative variable gene segment of the light chain of hFlex3a2 is entirely identical to its closest germline segment IGKV5-39*01 (Figure 1A). The high degree of similarity to its closest predicted germline progenitor suggests that immunizing mice with purified lipopolysaccharide (LPS) did not stimulate high levels of somatic mutation *in vivo.* The putative VH and VL genes were grafted onto the human IgG1 constant regions to create a chimeric huIgG1 and this antibody was confirmed by ELISA to bind to *S. flexneri* 3a outer membrane vesicles (OMVs) (Figure 1B), a proxy for the bacterial cell surface (38), as well as to coordinate complement-mediated bacteriolysis of *S. flexneri* 3a in a luminescent antibody bactericidal assay (L-ABA, Figure 1C). Additionally, hFlex3a2 was highly serotype-specific, binding to only the surface of *S. flexneri* 3a that expresses wildtype O-Ag, when screened against a panel of serotypes and an O-Ag knockout mutant (Figures S6A and 1D). Thus, the low level of somatic mutation, combined with its narrow breadth, make hFlex3a2 representative of a canonical mAb against a bacterial surface polysaccharide.

We sought to improve the affinity of hFlex3a2 against *S. flexneri* 3a O-Ag using phage display. Since hFlex3a2 would be displayed as an scFv, we wanted to confirm that the antibody retains functionality in this format. However, binding of *S. flexneri* 3a OMVs by hFlex3a2 in an scFv format could not be detected by ELISA (Figure 2A). This is not surprising, as scFvs often exhibit lower target affinity and are less stable than their IgG

139 counterparts (39,40). In an attempt to restore function to hFlex3a2 as an scFv, we
140 identified two residues in the framework region of the VH and one in the VL that were rare
141 and thus may be potentially problematic (41). We mutated all three of these residues to
142 the amino acid most frequently found at their respective positions when compared to a
143 database of other murine antibodies. We called this new mAb hFlex3a2_v2 (Figure 1A).
144 Two of these new mutations were away from the closest germline sequence, while the
145 other reverted that position back to its predicted germline amino acid (Figure 1A). As an
146 scFv, binding of hFlex3a2_v2 to *S. flexneri* 3a OMVs, but not to the unrelated antigen
147 ovalbumin, was observed (Figure 2A). Antigen binding was further confirmed by surface
148 staining, which demonstrated that hFlex3a2_v2 scFv, but not the original hFlex3a2 scFv
149 binds to the surface of *S. flexneri* 3a (Figure 2B). Importantly, as a chimeric huIgG1,
150 hFlex3a2_v2 exhibited antigen binding similar to the parent mAb, demonstrating that the
151 rare residues we identified did not impact IgG antibody binding (Figure 2C). Since
152 hFlex3a2_v2 retained binding as a huIgG1, and restored binding as an scFv, while
153 retaining antigen specificity, affinity maturation by phage display was completed using the
154 hFlex3a2_v2 background.
155
156 **Whole-cell in-solution panning enriched for mutations in the VL**
157 To test whether phage display can be used to identify single mutations that improve
158 hFlex3a2_v2 affinity, we designed two double-barcoded site-saturated mutagenesis
159 scanning libraries: one for VH and one for VL. Each library contained single amino acid
160 substitutions besides a cysteine at every site of either the VH or VL, leading to total library
161 sizes of 2,223 and 1,995 variants for the VH and VL libraries respectively. Flanking
162 synonymous codons were used to barcode mutation sites, enabling bioinformatic
163 identification of sampled positions for mutation enrichment analysis. Initial efforts to fix
164 purified *S. flexneri* 3a lipopolysaccharide to a plate for selection via solid-phase panning
165 were unsuccessful. Whole-cell in-solution panning was previously used to discover
166 antibodies that bind to bacterial surface carbohydrates (42), and so we adopted a similar
167 panning strategy for affinity maturing our existing O-Ag antibody (Figure 3A). The phage
168 display libraries were panned in solution for two rounds against either the target bacterium
169 *S. flexneri* 3a or *S. sonnei*, which is a closely related bacterium with an entirely different
170 O-Ag structure (43). Input and output page libraries were subsequently sequenced by
171 next-generation sequencing. We reasoned that variants enriched specifically after
172 panning against *S. flexneri 3a*, but not *S. sonnei*, were likely to exhibit improved binding
173 to the target relative to the parental mAb, and these variants could be evaluated further.
174 This approach also had some advantages over other panning strategies. Specifically, the
175 approach did not require large-scale purification of O-Ag, and the approach also allowed
176 for panning on O-Ag in its native conformation and abundance without any biochemical
177 modifications.
178
179 After two rounds of panning with the VH library, no enrichment of hFlex3a2_v2 variants
180 was detected (Figure S1A and S1B). In contrast, specific enrichment did occur for variants
181 in the VL library. Despite all the variants being of roughly equal abundance in the input
182 library, by the second round of panning, positively and negatively enriched variants were
183 identified when panned against *S. flexneri* 3a as well as *S. sonnei* (Figure 3B). After two
184 rounds of panning against *S. flexneri* 3a, a strong increase in the frequency of next-

generation sequencing reads for variant mutations mapping to residues that cluster around the VL CDRs was observed (Figure 3C). This enrichment was driven by the accumulation of reads mapping to either a single variant or a subset of variants at these sites (Figure S2). In some cases, such as at residue S30, a single variant was found to dominate relative to other variants with mutations at that site, while at other residues, such as N90, a few variants were found to be similarly abundant (Figure 3D). To determine whether highly enriched variants identified during phage display screening were of higher affinity than the parental antibody, we picked four variants — S30, L33, A51, and N90 — for further investigation. We chose these variants because all four had large increases in read frequencies after panning, suggesting that these residues may be important. Additionally, each variant was specifically enriched following panning against *S. flexneri* 3a relative to *S. sonnei* (Figures 3E and S3 and Table 1). Lastly, these variants are located in or adjacent to CDRL1 (S30 and L33), CDRL2 (A51) or CDRL3 (N90). Since no variants in the VH were enriched for, we will refer to the hFlex3a2_v2 variants solely by their VL mutation(s) from here on.

Variants enriched in phage display improve mAb binding to *S. flexneri* 3a O-Ag as chimeric huIgG1s

We hypothesized that the selected variants of hFlex3a2_v2 that were highly enriched against *S. flexneri* 3a but not *S. sonnei* (S30G, L33N, A51R, and N90H) were likely to have genuinely higher affinity against *S. flexneri* 3a O-Ag relative to the parent mAb. For a comparison, we chose one additional variant — H34A — that was highly enriched against both *S. flexneri* 3a and *S. sonnei* (Figures 3D, 3E, S3, and Table 1). All the selected variants were produced as chimeric huIgG1s for further characterization (Table 1).

Surface staining showed that all the variants retained their ability to bind to the surface of *S. flexneri* 3a (Figure 4A). Titration ELISA also confirmed binding to *S. flexneri* 3a OMVs (Figure 4B) and showed that all four of the variants that were specifically enriched against *S. flexneri* 3a (S30G, L33N, A51R, and N90H) had higher apparent affinities than their parental mAb hFlex3a2_v2, while the variant that was enriched against both *S. flexneri* 3a and *S. sonnei* (H34A) had a lower apparent affinity (Figure S4A). The ELISA binding curves were used to calculate EC_{50s} (Table 1 and Figure 4C). The parent mAb hFlex3a2_v2 had an EC_{50} of 57.81 nM. L33N, the variant with the highest apparent affinity, had an EC_{50} of 4.99 nM, while variant H34A had the lowest apparent affinity (EC_{50} 205.09 nM). This is consistent with the hypothesis underlying our panning strategy, that specific enrichment against *S. flexneri* 3a provides a means of identifying variants that improve target affinity.

We next wanted to determine whether combining the most beneficial single amino acid mutations — S30G, L33N, and A51R — would synergize with one another to further improve the affinity of hFlex3a2_v2. We constructed all the possible double and triple combinatorial mutants. Since all the combinatorial variants retained their ability to bind *S. flexneri* 3a (Figure 4A), we performed ELISA to determine their apparent affinities. All of the combinatorial variants except L33N + A51R had synergistic improvements in apparent affinity, meaning that the combinatorial variant had a lower EC_{50} than that of any single

231 mutation contained in the combination (Table 1, and Figures 4B, 4C, and S4A). Variant
232 S30G + L33N was the most potent binder, with an EC_{50} = 2.56 nM. We also tested a
233 variant combining all 5 of the single mutations and found that its apparent affinity (EC_{50} =
234 201.35 nM) was similar to that of H34A alone, suggesting that the presence of mutation
235 H34A may be dominantly detrimental over the other beneficial mutations. Due to the
236 oligomeric structure of O-Ag, it is difficult to accurately measure its molar concentration
237 in solution, complicating efforts to precisely measure the binding kinetics between the
238 mAbs and purified O-Ag *in vitro*. However, biolayer interferometry (BLI) confirmed that
239 the parent mAb, and the most potent and least potent variants in ELISA, S30G + L33N
240 and H34A respectively, can all bind purified *S. flexneri* 3a O-Ag (Figure 4D). Consistent
241 with the selected mutations affecting binding behavior, at both concentrations of O-Ag
242 tested, S30G + L33N reached a higher plateau in BLI than the parental mAb, while H34A
243 reached a lower plateau. Lastly, a panel of polyspecificity reagents were used in ELISA
244 to demonstrate that the mAb variants had limited polyreactivity against the antigens
245 tested, confirming that the better binding variants retained their antigen specificity (Figure
246 S4B).
247
248 **Improving binding of hFlex3a2_v2 enhances effector and anti-virulence functions**
249 To probe the relationship between improved O-Ag affinity and potency across
250 antibacterial functions, we tested our panel of hFlex3a2 variants in a series of effector
251 function and virulence assays. A Luminescent Antibody Bactericidal Assay (L-ABA),
252 which measures the ability of antibodies to coordinate complement-mediated
253 bacteriolysis, showed that the parent antibody was already potent at this effector function
254 (IC_{50} = 1.86 nM, Table 1, Figures 5A and S5A). Nonetheless, the best binding single
255 amino acid variant, L33N, modestly but reproducibly improved upon the parent mAb
256 (IC_{50}= 1.32 nM, p=0.04), while the best binding combinatorial variant, S30G + L33N, had
257 a more substantial ~2.7-fold improvement in potency (IC_{50} = 0.68 nM, p<0.0001). The
258 worst binding variant H34A had the weakest potency in L-ABA (IC_{50} = 4.86 nM, p<0.0001),
259 showing that binding strength and *in vitro* complement-mediated bacteriolysis are
260 correlated (R^2=0.91, Figure S5B). Similarly, when hFlex3a2_v2 was tested in a
261 complement-independent opsonophagocytosis assay (OPA) at a 30 nM concentration,
262 17.7% of monocytes were cell trace violet positive (CTV+), indicating that they had
263 phagocytosed *S. flexneri* 3a that was opsonized with this mAb (Figure 5B). The gating
264 strategy for OPA is shown in Figure S4C. Although hFlex3a2_v2 already had the ability
265 to facilitate OPA activity, L33N, the best binding single amino acid variant, was almost 2-
266 fold more potent at the same concentration (33.7% CTV+, p = 0.02). The best binding
267 combinatorial variant S30G + L33N was the most potent at facilitating OPA (38.6% CTV+,
268 p <0.005). Despite having little improvement in binding and L-ABA compared to the
269 parental mAb, variant N90H was the third most potent in OPA (32.2% CTV+, p = 0.04).
270 Similarly, despite exhibiting lower apparent affinity, H34A and the combination of all 5
271 mutations had similar potency in OPA to the parent antibody at 30 nM (Figure 5B). This
272 demonstrates that, while largely correlated, other factors beyond binding strength also
273 impact O-Ag mAb function in the OPA.
274
275 In addition to promoting effector functions that modulate the immune system, mAbs can
276 also directly neutralize bacterial virulence. As an intracellular pathogen, invasion of

colonic epithelial cells is an indispensable step in the pathogenesis of *S. flexneri*. An *in vitro* invasion assay showed that, relative to PBS or a non-binding control mAb, hFlex3a2_v2 does not significantly block *S. flexneri* 3a invasion of a monolayer of HeLa cells (Figure 5C). However, the highest affinity single amino acid variants and combinatorial variants all blocked *S. flexneri* 3a invasion by at least 60% (Figure 5C). This demonstrates that for anti-O-Ag antibodies, increasing affinity can help to directly neutralize bacterial virulence.

Improving affinity of hFlex3a2_v2 against *S. flexneri* 3a increases its functional potency against *S. flexneri* 3b

Lastly, we wanted to determine whether higher affinity variants of hFlex3a2_v2 would also have increased breadth compared to their parent mAb. Although the precise epitope of hFlex3a2_v2 is not known, we reasoned that many of the components of *S. flexneri* 3a O-Ag are also found in the O-Ag of other *S. flexneri* serotypes, and some of the variants may have increased affinity against some O-Ag component common to other *S. flexneri* serotypes. We performed a surface staining experiment with a panel of *S. flexneri* serotypes that all share the same core O-Ag sugars, but with different modifications, as well as *S. sonnei*, which has an entirely unrelated O-Ag composition (Figure 6A). As previously shown, all hFlex3a2_v2 variants bound to *S. flexneri* 3a and binding to a mutant *S. flexneri* 3a O-Ag- strain (Figure S6A) was 10-fold lower than to *S. flexneri* 3a that expresses wildtype O-Ag, confirming that O-Ag is necessary for binding. For all the hFlex3a2 variants tested, no reactivity to *S. flexneri* serotypes 1b, 2a, 2b, Y, or *S. sonnei* was observed (Figure 6B). In contrast, surface staining against *S. flexneri* 3b showed that hFlex3a2_v2 weakly cross-reacts with this serotype. The single amino acid variant L33N and the combinatorial variant S30G + L33N had surface staining median fluorescence intensities that were 4-fold and 5.7-fold higher, respectively.

Since surface staining experiments showed that the higher affinity variants of hFlex3a2_v2 bind to *S. flexneri* 3b, we wanted to further characterize their effect on binding and effector function. ELISA measuring binding to *S. flexneri* 3b OMVs, in agreement with the surface staining experiment, showed that hFlex3a2 weakly binds to *S. flexneri* 3b O-Ag (Figure 6C and Figure S6B). The variants showed the same pattern in relative apparent affinities as against *S. flexneri* 3a. Specifically, single amino acid variants S30G, L33N, and A51R all increased apparent affinity. N90H bound similarly to the parent antibody and H34A had a lower apparent affinity than the parent antibody. All combinations of the beneficial single mutations were found to be synergistic except for L33N + A51R. The combination of all 5 mutations bound poorly, similarly to H34A alone. The best binding single mutation was L33N, and the best binding combinatorial mutation was S30G + L33N, which had EC_{50} values of 322.5 nM and 165.3 nM respectively. We next wanted to determine whether these improvements in affinity for *S. flexneri* 3b O-Ag are sufficient to drive effector functions against this serotype. We compared the parent mAb to the best binding single variant, L33N, and the best binding combinatorial variant, S30G + L33N, in an L-ABA assay. In this assay, hFlex3a2_v2 displayed weak complement-mediated bactericidal activity against serotype 3b, only reaching 37% killing at 90 nM, the highest concentration of antibody tested (Figure 6D). Both the single L33N mutation and combination of S30G + L33N mutations were more potent in this assay, with

323 IC_{50} values of 30.4 nM and 18.0 nM, respectively. Similarly, in an OPA assay,
324 hFlex3a2_v2 was able to facilitate opsonophagocytosis at a concentration of 30 nM,
325 leading to 7.4% CTV+ monocytes (Figure 6E). At the same concentration of mAb, the
326 most potent single amino acid variants were ~3-fold more potent at OPA, while the most
327 potent combinatorial variants were ~4.5-fold more potent (Figure 6E). However, despite
328 improving affinity and potency in effector function assays, the higher affinity variants of
329 hFlex3a2_v2 did not block *S. flexneri* 3b invasion (Figure 6F). Together, this data shows
330 that panning against *S. flexneri* 3a was able to increase the functional breadth of this
331 antibody to also exhibit effector functions against *S. flexneri* 3b, likely by improving the
332 affinity to a shared epitope on these two serotypes that was weakly recognized by the
333 parent mAb.
334
335 **Discussion**
336 Here, we report the development of a panning strategy that enabled the rapid affinity
337 maturation of a mAb against the O-Ag of *S. flexneri* 3a. We demonstrate that variants with
338 improved affinity exhibit more potent effector functions against both *S. flexneri* 3a and the
339 related but distinct serotype *S. flexneri* 3b. By pairing whole-cell in-solution panning with
340 NGS and using both the target bacterial strain and a related strain with a completely
341 unrelated O-Ag, we were able to efficiently identify specific mutations that could increase
342 affinity against the target strain. It is notable that out of the four tested variants that met
343 the criteria for specific enrichment (S30G, L33N, A51R, and N90H), three of them (S30G,
344 L33N, A51R) improved affinity by ELISA, and all four exhibited improved potency in at
345 least one effector function assay. One of these mutations, L33N, was sufficient to
346 increase apparent affinity in ELISA by approximately 10-fold over the parent mAb, which
347 is comparable to what has been reported for germline mAbs against *Chlamydia* core
348 lipopolysaccharide (28). In contrast, H34A, which was enriched against both bacterial
349 species (possibly indicating that this mutation improves a non-specific parameter such as
350 display efficiency on phage), had lower affinity than the parent, supporting the rationale
351 of this approach.
352
353 Unexpectedly, while variants in the hFlex3a2 VL library were successfully enriched
354 following panning, no variants were enriched from the VH library (Figure S1). It is possible
355 that the VH is already optimized, and we were simply unable to find point mutations that
356 conferred additional advantage. This is supported by the observation that, while the VL
357 protein sequence of hFlex3a2 is identical to germline, the VH sequence already contains
358 somatic mutations that result in four amino acid substitutions (Figure 1A). However, the
359 fact that no enrichment was observed against either *S. flexneri* 3a or *S. sonnei* (which
360 would not be expected, as at least some variants should be nonspecifically enriched for
361 reasons of improved display efficiency or scFv stability), leaves open the possibility that
362 this was a technical issue with the panning process rather than a biological one. Further
363 experiments would be needed to definitively determine whether any additional VH
364 mutations can further improve binding and function of hFlex3a2. The identification and
365 characterization of VH mutations that further synergize with the already identified VL
366 mutations will be of interest in future studies.
367

368 As expected, higher affinity hFlex3a2 variants were generally more potent across all
369 assays (Figure 5), with some notable exceptions. In L-ABA, affinity was tightly correlated
370 with potency (Figure S5B), suggesting that potency in this assay has a linear relationship
371 with affinity. Similarly, higher affinity variants were able to block invasion by *S. flexneri* 3a,
372 while the parent mAb was not (Figure 5C). However, even these enhanced variants were
373 unable to block invasion by serotype 3b (Figure 6F). While it is possible that the
374 mechanism of action by which hFlex3a2 and its variants are inhibiting *S. flexneri* 3a
375 invasion is not applicable to *S. flexneri* 3b, we suspect that this observation is more likely
376 due to invasion inhibition requiring a greater affinity than L-ABA or OPA activity. Even
377 though some hFlex3a2_v2 variants are more potent against *S. flexneri* 3b than the
378 parental mAb, the best variants have weaker affinity and potency against serotype 3b
379 than 3a. Given the inherent biological variability of the invasion assay compared to L-ABA
380 or OPA, and that the parent mAb does not measurably inhibit invasion against even 3a,
381 we think that the best variants simply lack sufficient affinity to reach the threshold where
382 a decrease in invasion by 3b is consistently measurable in this assay. It is possible that
383 panning against 3b with the hFlex3a2_v2 library would identify variants that further
384 improve activity against this serotype.
385
386 The relationship between OPA and affinity was more complex than those between affinity
387 and the L-ABA or invasion assay. While the highest affinity variants tested here (L33N
388 and S30G + L33N) did exhibit higher degrees of opsonophagocytosis than the parent
389 mAb, N90H, which does not have detectably higher affinity and was not more potent in
390 L-ABA, also improved macrophage uptake of both *S. flexneri* 3a and 3b (Figure 5B and
391 6E). Similarly, H34A, which has lower affinity and L-ABA potency than the parent,
392 performed similarly to the parent mAb in the OPA (Figure 5B and 6E). A similar
393 phenomenon has been observed for some mAbs targeting the human immunodeficiency
394 virus (HIV) glycoprotein gp120 as they exhibit different capacities to drive antibody-
395 dependent cellular cytotoxicity against HIV-infected cells displaying gp120, despite being
396 from the same lineage, having the same affinity, and binding the same epitope (44). In
397 that study, it was proposed that these differences are a consequence of either subtle
398 variations in the structural recognition of the epitope or other changes in the binding
399 dynamics between the mAb and the antigen. We suspect similar factors, such as changes
400 in the kinetics of binding (but not necessarily equilibrium affinity) may allow N90H to
401 coordinate opsonophagocytosis more efficiently than the parent mAb despite having the
402 same apparent equilibrium affinity. Unfortunately, because purified *S. flexneri* 3a O-Ag is
403 present at a range of molecular weights, it is not currently possible to obtain accurate
404 kinetic measurements to test this hypothesis. However, future studies on the relationship
405 between affinity and effector function potency among mAbs against bacterial
406 polysaccharides may provide more mechanistic insights. Altogether, these data support
407 the hypothesis that higher affinity generally improves antibacterial function performance
408 for anti-O-Ag mAbs, with some notable exceptions and potential caveats.
409
410 Most importantly, this work informs the development of therapeutic mAbs targeting
411 bacterial polysaccharides. More test cases are required to establish the generalizability
412 of this approach. However, these data demonstrate that in principle, this whole-cell in-
413 solution panning approach can rapidly identify variants with improved affinity without the

414 need for antigen purification, and these improvements lead to direct functional
415 improvements. More interestingly, the observed enhancement of activity against *S.*
416 *flexneri* 3b suggests that if a mAb is targeting an epitope shared with other bacterial
417 serotypes, it may be possible to improve functional breadth alongside potency. This
418 supports the development of clinically relevant mAbs against bacterial polysaccharides,
419 because discovery campaigns can now prioritize mAbs that have relatively high breadth
420 by binding sugars common to many bacterial polysaccharides. Broad binders can then
421 be rapidly improved using this method. Future work will explore the potential of more
422 complex panning strategies that incorporate multiple serotypes, which can further
423 facilitate the identification of variants with improved breadth. Altogether, these results are
424 an important step towards expanding the mAb engineering toolkit for anti-polysaccharide
425 mAbs, which in turn may help develop novel therapeutics against AMR bacterial
426 pathogens.
427
428 **Materials and methods**
429 **Bacterial strains and growth conditions**
430 Bacterial strains and plasmids used in this study can be found in Table S2. *Shigella* strains
431 were maintained at -80 °C in tryptic soy broth (TSB) containing 20% (vol/vol) glycerol.
432 *Shigella* was grown aerobically at 37 °C on TSB agar with 0.01% Congo red dye.
433 For all assays, bacteria were grown in the desired medium overnight, then subcultured
434 1:100 into fresh growth medium and grown aerobically at 250 rpm, 37 °C.
435
436 **Cell culture conditions**
437 HeLa cells were grown in high glucose DMEM (Gibco) + 10% FBS + 2 mM glutamine and
438 1x Pen/Strep. THP-1 cells were grown in RPMI (Gibco) + 10% FBS + 10mM Hepes pH
439 7.4 + 1 mM Sodium Pyruvate + 55 µM beta-mercaptoethanol and 1x Pen/Strep. For
440 assays involving bacteria, HeLa and THP-1 cells were first washed into fresh media that
441 does not contain Pen/Strep. Expi293™ cells were grown in Expi 293™ Expression
442 Medium (Gibco).
443
444 **10x sequencing of hybridomas**
445 An unsequenced hybridoma expressing the mAb hFlex3a2, which was discovered and
446 described previously by WRAIR and collaborators (37), was provided to IAVI by WRAIR.
447 Single cells were isolated using a BD FACSMelody™ cell sorter, and heavy and light
448 chain variable domains were sequenced using the 10X single cell genomics platform (10X
449 Genomics, Inc.). Sequence analysis to predict CDRs, align to germline, and identify rare
450 residues was done using IMGT/V-Quest, IgBLAST, and abYsis (45–47). The VH and VL
451 sequences were cloned into a modified pcDNA3.2 expression vector and purified as full
452 IgG as described below. The mAb was confirmed to have properties consistent with the
453 parental hybridoma mAb (Figure 1).
454
455 **Construction of plasmids**
456 Primers and plasmids used in this study can be found in Table S3. For periplasmic
457 expression of scFvs, hFlex3a2 and hFlex3a2_v2 were designed as scFvs in the following
458 orientation — PelB signal sequence, hFlex3a2 VH, (GGGGS)3X linker, hFlex3a2 VL —
459 ordered as gBlocks (Integrated DNA Technologies), then cloned between the NcoI and

460 BamHI restriction sites of the bacterial expression vector pET28b (+) using NEBuilder®
461 HiFi DNA Assembly following the manufacturer's instructions (New England Biolabs). For
462 expression as huIgG1, the variable regions of hFlex3a2 and hFlex3a2_v2 were cloned
463 into a pcDNA3.2-based human antibody expression vectors containing the relevant
464 huIgG1 or Ig kappa constant domains. For single amino acid mAb variants, primers were
465 designed to insert the mutations into the appropriate VL sequence by HiFi DNA Assembly
466 (New England BioLabs). Combinatorial variants of hFlex3a2 and hFlex3a2_v2 VL chains
467 were ordered as gBlocks and inserted into the appropriate human antibody expression
468 vector using NEBuilder® HiFi assembly.
469
470 **Construction of *Shigella* mutants**
471 *Shigella flexneri* 3a and 3b *tolR* mutants that hyperproduce OMVs (48), and *S. flexneri* 3a
472 *waaL* mutant (O-Ag knockout) (49) were produced by the gene-gorging method as
473 previously described (50). Briefly, a mutation cassette consisting of 500 bp of *Shigella*
474 genomic DNA upstream of the target mutation site, the kanamycin resistance gene from
475 plasmid pKD4, and 500 bp of DNA downstream of the target mutation site, flanked on
476 both sides of the mutation cassette by the restriction site I-SceI was constructed using
477 splice by overlap extension PCR (51). The mutation cassette was A-tailed and ligated into
478 the plasmid pGEM®-T Easy (Promega) to create a donor plasmid. The donor plasmid
479 was electroporated into the desired *S. flexneri* strain that had previously been
480 electroporated with plasmid pACBSR. Strains containing both the donor plasmid and
481 pACBSR were grown for 6 hours at 30 °C in LB + chloramphenicol + 0.4% arabinose to
482 induce genomic recombination and then plated on TSBA + Kanamycin for single colonies.
483 Colonies were passaged multiple times at 37 °C to promote the loss of pACBSR. After
484 multiple passages, colonies were confirmed to be kanamycin resistant but
485 chloramphenicol sensitive, indicating loss of donor plasmid, and the successful insertion
486 of the genomic mutation was verified by Sanger sequencing.
487
488 **Phage library construction and panning**
489 Double-barcoded site-saturated mutagenesis scanning libraries of the VL and VH of
490 hFlex3a2_v2 were designed and ordered from Twist Biosciences. The libraries were
491 amplified with primers to introduce SfiI sites and then ligated into the SfiI site of phagemid
492 pCOMB3XSS (52). To produce phage, the phagemid libraries were electroporated into
493 XL1-Blue (Agilent), recovered in 5 mL of SOC, and then grown (37 °C, 250 RPM) to OD_{600}
494 ~0.5 in 10 mL of Super Broth + Tet + Carb before being super infected with M13ko7 helper
495 phage (New England Biosciences) at an MOI of 20, expanded, and grown overnight (30
496 °C, 250 rpm) in 200 mL of super broth + Tet + Carb + Kan.
497
498 Phage was precipitated from the supernatant with 0.5 M NaCl and 4% PEG-8,000 as
499 previously described (53) and then panned against whole bacteria in-solution, based on
500 a previously published method (42). Briefly, 1 x 10^9 cfu of *S. flexneri* 3a or *S. sonnei* were
501 blocked in 3% nonfat milk in PBS and then each bacterial species was incubated with 5
502 x 10^{10} pfu of blocked phage particles for 15 min to 2 h. Non-binding phage was washed
503 5x with PBS + 5% Tween-20 after round 1 of panning and washed 10x after round 2.
504 Binding phage was eluted by mixing with 0.1 M HCl pH 2.2 (pH adjusted with glycine) for
505 ten minutes at room temperature, then neutralized with 2 M Tris base and used to reinfect

506 XL1-Blue cells to generate phage for the second round of panning. XL1-Blue containing
507 the input library, post-panning round 1 phagemids, and post-panning round 2 phagemids
508 were maxiprepped, the variable chain sequences were PCR-amplified and deep-
509 sequenced by MiSeq (Illumina) using Amplicon-EZ platform (Genewiz). The relative
510 enrichment of phage library variants against *S. flexneri* 3A and *S. sonnei* after rounds 1
511 and 2 of panning was quantified using an in-house Python script.
512
513 **Antibody and antigen purification**
514 For purification of IgGs, Expi293 cells were co-transfected with the desired heavy chain
515 and light chain pair at a ratio of 1:2.5 with FectoPRO® (Polyplus) in Expi293™ Expression
516 Medium (Gibco). The cells were supplemented with 3 mM valproic acid (Sigma-Aldrich)
517 and 0.4% D-(+)- glucose (Sigma-Aldrich) 24 h after transfection. The supernatant was
518 harvested on day 5 post-transfection, IgGs were purified using Praesto AP+ agarose resin
519 (Purolite), and then buffer exchanged and concentrated using 30 kDa cutoff spin filter
520 (Amicon).
521
522 scFv purification was based on a previously described method (54). Briefly, BL21
523 containing the desired scFv cloned into pET28b (+) was grown to OD_{600} 0.6-0.8 in terrific
524 broth (37 °C, 250 rpm) and then induced with 1 mM IPTG overnight (18 °C, 250 RPM).
525 Bacteria were collected, resuspended in 40 mL of TES buffer (0.5 M Sucrose, 0.5 mM
526 EDTA, and 0.2 M Tris-HCl pH 8.0), incubated at 4 °C for 30 min, and then osmotically
527 shocked with 80 mL of ice-cold ddH_2O for 1 h at 4 °C. Lysed bacteria were pelleted, the
528 supernatant was collected, adjusted to 150 mM NaCl, 2 mM $MgCl_2$, 20 mM imidizaole,
529 and incubated with 1 mL of Ni-NTA resin (Anatrace) at 4 °C for at least 1.5 h. scFv bound
530 resin was packed onto gravity columns, washed extensively with wash buffer (150 mM
531 NaCl, 2 mM $MgCl_2$, 30 mM imidazole), and then eluted with elution buffer (150 mM NaCl,
532 2 mM $MgCl_2$, 300 mM imidazole) before buffer exchanging and concentrating with PBS
533 using a 10 kDa cutoff centrifugal filter (Amicon).
534
535 To purify OMVs, supernatant was collected from *S. flexneri* 3a or 3b tolR::kan mutants
536 grown overnight in SSDM (48) supplemented with 40 mg/L l-methionine and 20 mg/L
537 tryptophan. The supernatant was filter-sterilized through a 0.2 µM filter (Sartorius) and
538 then concentrated to ~ 50 mL by tangential flow filtration using a Vivaflow® 100 kDa cutoff
539 filter (Sartorius®). The concentrated supernatant was ultracentrifuged at 200,000 x g for
540 1.5 h to pellet OMVs, which were then resuspended in 1 mL of PBS and stored at -20 °C
541 for future use. Total protein content of OMVs was quantified by Micro-BCA™ assay
542 (Thermo Fisher) following the manufacturer's instructions. OMV amount was normalized
543 by total protein content for ELISA assays.
544
545 O-Ag was purified from whole bacteria by acetic acid hydrolysis (55). Acetic acid was
546 added at a final concentration of 2% to a culture of stationary phase *S. flexneri* 3a and
547 incubated at 100 °C for 5 h. After hydrolysis, the culture was neutralized to pH ~ 6 with
548 ammonium hydroxide (Sigma-Aldrich). Bacterial debris was pelleted, the supernatant was
549 buffer exchanged by tangential flow filtration using a VivaFlow 30 kDa cutoff filter
550 (Sartorius) first into 1 M NaCl, and then into ddH_2O.The buffer exchanged supernatant
551 was concentrated to ~50 mL. Citrate buffer (20 mM, pH 3) was added to the supernatant,

552 and it was incubated at room temperature for 30 min, centrifuged at 12,000 x g for 30 min
553 and then passed through a Sartobind® IEX S75 cationic exchange filter (Sartorius). After
554 cation exchange, the supernatant was precipitated once more with 18 mM Na_2HPO_4, 24%
555 ethanol, and 200 mM $CaCl_2$ at room temperature for 30 min, then buffer exchanged as
556 described above before being concentrated to approximately 1 mL in ddH_2O using a 30
557 kDa cutoff spin filter (Amicon). The purified O-Ag was quantified using a Total
558 Carbohydrate Assay Kit (Sigma-Aldrich) following the manufacturer's instructions.
559 Contaminating DNA and protein levels were assessed by nanodrop analysis and Micro-
560 BCA™ assay, respectively, and confirmed to be at least 10-fold lower than carbohydrate
561 concentration.
562
563 **ELISA assays**
564 All ELISA assays were performed in 384-well high binding ELISA plates (Corning). Wells
565 were coated overnight at 4 °C with antigen in PBS at a concentration of 2.5 µg/mL for
566 OMVs or 5 µg/mL for ovalbumin, CHO-SMP, insulin, and ssDNA. Antigen-coated wells
567 were blocked in PBS containing 3% BSA and 0.05% Tween-20 at 37 °C for 1 h. Antibodies
568 to be tested were diluted in 1% BSA + 0.017% Tween-20 at the desired antibody
569 concentration and incubated with the blocked antigen at 37 °C for 1 h. After incubation
570 with the test antibody, wells were washed 3x with PBS + 0.05% Tween-20 and incubated
571 with the appropriate secondary antibody at room temperature for 1 h. Secondary
572 antibodies used were either AP-conjugated anti-Flag M2 (Sigma-Aldrich) for scFvs or AP-
573 conjugated anti-Human Fc (Jackson ImmunoResearch) for huIgG1s, both at a 1:1000
574 dilution in PBS + 1% BSA + 0.017% Tween-20. After washing three times more, AP
575 substrate tablets (Sigma-Adrich) were dissolved and diluted to 1 mg/mL in AP buffer (50
576 mM $MgCl_2$, 100 mM NaCl, 1%Tween 20). ELISAs were developed with AP substrate (20
577 min for IgGs or 40 min for scFvs) at room temperature. Absorbance at 405 nm was read
578 on a BioTek Synergy microplate reader.
579
580 **Luminescent Antibody Bactericidal Assays (L-ABA)**
581 L-ABA was adapted from previously published protocols (37,56). Briefly, the desired *S.*
582 *flexneri* serotype was grown to mid-log phase in TSB (BD Biosciences) and resuspended
583 at a concentration of 3 x 10^5 CFU/mL in 100 µL of assay buffer (HBSS + 0.1% Gelatin,
584 pH 7.4) with 7.5% Baby Rabbit Complement (Pel-Freez Biologicals), and the test antibody
585 at the desired concentration. The L-ABA reaction was incubated for 3 h at 37 °C, washed
586 once with 100 µL of fresh assay buffer, mixed 1:1 with BacTiter-Glo™ (Promega), and
587 incubated for 5 min at room temperature. Luminescence was read on a BioTek Synergy
588 plate reader. Adalimumab (57) expressed as a chimeric macaque IgG1 was used as a
589 control mAb. To normalize for differences in bacterial growth, the data was fit with a
590 sigmoidal four parameter logistic curve on GraphPad Prism. Each curve was normalized
591 to the Top best-fit value of their curve to determine their fraction maximal luminescence.
592 Control mAb values are normalized to the luminescence signal of total bacterial growth in
593 assay buffer and baby rabbit complement.
594
595 **Opsonophagocytosis Assays (OPA)**
596 For OPA, the desired *S. flexneri* strain was grown to OD_{600} of approximately 0.5 in TSB,
597 washed with PBS, and stained with a 1:50 dilution of CellTrace™ Violet (CTV, Thermo

598 Fisher) for 15 min at 37 °C. Excess dye was quenched with FACS buffer (PBS + 1%
599 FBS), the bacteria were washed in PBS and resuspended in assay buffer (HBSS + 0.1%
600 gelatin, pH 7.4). 2.5 x 10^6 CFU of bacteria were mixed with the desired concentration of
601 mAb in assay buffer and incubated at 37 °C for 30 min. Opsonized bacteria were then
602 mixed with 5 x 10^4 THP-1 cells and incubated for 30 min at 37 °C in 5% CO_2. After 30
603 min, the OPA reactions were stained on ice in the dark for 30 min with Live/Dead Near-
604 IR dye (Thermo Fisher) diluted 1:2000 in PBS and FITC-conjugated anti-CD45 antibody
605 (BD Biosciences) diluted 1:4000. The cells were then fixed with 4% PFA for 30 min, on
606 ice. To determine relative OPA activity, the percentage of THP-1 cells incubated with *S.*
607 *flexneri* opsonized with the mAbs of interest that were Near IR-, CD45+, and CTV+ was
608 quantified by flow cytometry using a FACSCelesta (BD Biosciences).
609
610 **Invasion Assays**
611 Invasion was measured by a gentamicin protection assay (58). *S. flexneri* was grown to
612 an OD_{600} of approximately 0.7 in TSB (37 °C, 250 RPM), washed in PBS, resuspended
613 at a concentration of 1 x 10^9 CFU/mL, and incubated with 1 µM of the desired mAb or
614 PBS (control) for 30 min at 37 °C. 10 µL of bacteria (~1 x 10^7 CFU, MOI = 20) was added
615 to a monolayer of approximately 5 x 10^5 HeLa cells in a tissue culture-treated 24-well
616 plate (Corning) and centrifuged at 900 x g for 10 min. The plate was incubated for 30 min
617 at 37 °C and 5% CO_2, washed two times with PBS, the media was replaced with DMEM
618 containing 25 µg/mL gentamicin, and the plate was incubated for an additional 1 h. The
619 wells were washed twice more with PBS and then lysed with 0.1% Triton X-100. Serial
620 dilutions of the mAb-treated and control bacteria were plated, and percent invasion was
621 calculated. Adalimumab (57) expressed as a chimeric macaque IgG1 was used as a
622 control mAb.
623
624 **Bacterial surface staining**
625 To measure bacterial surface staining, *S. flexneri* was grown to an OD_{600} of approximately
626 0.5, washed and resuspended in PBS to a concentration of 2 x 10^9 CFU/mL. The desired
627 mAb was added to 25 µL of bacteria at a final concentration of 50 nM and incubated at
628 37 °C for 30 min. The bacteria were washed with PBS and then incubated with a 1:100
629 dilution of the appropriate secondary antibody for 30 min at room temperature. For scFvs,
630 the secondary antibody was Alexa Fluor 647-conjugated anti-Flag antibody (Abcam), and
631 for huIgGs this was BV421-conjugated anti-Human IgG (BD Biosciences). Bacteria were
632 then fixed with 4% PFA for 30 min on ice. Median fluorescence intensity was determined
633 by flow cytometry on a FACSSymphony A5 (BD Biosciences).
634
635 **Biolayer interferometry**
636 Binding of hFLex3a2_v2 variants to *S. flexneri* 3a O-Ag was characterized by BLI using
637 an Octet® R8 (Sartorius) with Octet AHC Biosensors (Sartorius). All antibodies and
638 antigens were in PBS + 0.02% Tween-20 + 0.01% BSA. The BLI protocol was as follows:
639 300 seconds baseline, 120 seconds loading with 1 µM mAb, 180 seconds baseline, 360
640 seconds association with 100 µg/mL of *S. flexneri* 3a O-Ag or 540 seconds with 20 µg/mL
641 of *S. flexnei* 3a O-Ag, and 600 seconds dissociation. BLI results were analyzed on Octet
642 Analysis Studio (Sartorius) and plotted with GraphPad Prism. hFlex2a1 (37) expressed
643 as a chimeric huIgG1 was used as a control mAb.

644
645 **O-Ag visualization**
646 To visualize O-Ag, crude protein-free LPS extract was purified from *S. flexneri* 3a and *S.*
647 *flexneri* 3a waaL::kan (O-Ag-) following the method of Darveau and Hancock (59).
648 Bacterial LPS extract was separated by SDS-PAGE and stained with Pro-Q™ Emerald
649 300 Lipopolysaccharide Gel Stain Kit (Thermo Fisher) following the manufacturer's
650 instructions. Stained gels were visualized on a ChemiDoc MP Imaging System (Bio-Rad).
651
652 **Fig 1: Analysis of binding and function of putative hFlex3a2 as a huIgG1 chimera.**
653 (A) Alignment of putative hFlex3a2 VH and VL protein sequences to their closest germline
654 progenitors shows high levels of similarity. Residues that were modified to create mAb
655 hFlex3a2_v2 are denoted by (*). Alignment and CDR predictions were determined with
656 IMGT/V-Quest and rare residues were identified with abYsis (45,46). (B) Titration ELISA
657 measures the binding of increasing concentrations of hFlex3a2 huIgG1 to 2.5 μg/mL of
658 *S. flexneri* 3a OMVs. This experiment is the average of three independent replicates each
659 performed in duplicate. (C) L-ABA measuring the ability of increasing concentrations of
660 hFlex3a2 huIgG1 and a non-binding control mAb, to coordinate complement-mediated
661 bacterial killing of *S. flexneri* 3a. L-ABA is the average of three biological replicates
662 performed in duplicate. (D) Surface staining with 50 nM of mAb shows that hFlex3a2, and
663 not a non-binding control mAb, binds specifically to *S. flexneri* 3a wildtype O-Ag. This
664 experiment is the average of three experimental replicates. Error bars represent standard
665 deviation.
666
667 **Fig 2: Analysis of binding of hFlex3a2 and hFlex3a2_v2 as an scFv.** (A) Titration
668 ELISA shows that at concentrations above 100 nM of scFv, hFlex3a2_v2, but not
669 hFlex3a2, binds to *S. flexneri* 3a OMVs (2.5 μg/mL). Neither scFv bound to the unrelated
670 antigen ovalbumin (5 μg/mL). This experiment was repeated three times, and a
671 representative experiment is shown. (B) Titration ELISA of hFlex3a2_v2 reformatted as
672 a chimeric huIgG1 and the original hFlex3a2 huIgG1 shows similar binding to *S. flexneri*
673 3a OMVs (2.5 μg/mL). This experiment is the result of two independent replicates. (C)
674 Surface staining confirms that in the scFv format, hFlex3a2_v2, but not hFlex3a2, binds
675 *S. flexneri* 3a. scFvs were tested at a concentration of 1μM. This experiment represents
676 two replicates. Error bars represent standard deviation.
677
678 **Fig 3: Whole-cell in-solution panning enriches for VL variants.** (A) Whole-cell in-
679 solution panning strategy. To identify better binding variants of hFlex3a2_v2 scFv, we
680 panned a phage-displayed site-saturated mutagenesis scanning library of VL or VH
681 against either *S. flexneri* 3a or *S. sonnei* in-solution for two rounds and sequenced output
682 phage by next-generation sequencing to identify variants that were specifically enriched
683 against *S. flexneri* 3a. (B) log10 enrichment of variants in the VL library after two rounds
684 of panning against *S. flexneri* 3a and *S. sonnei*. Dotted line is 20 standard deviations
685 above the mean mutation enrichment in the input library and indicates a stringent
686 threshold set to distinguish bacteria-mediated enrichment from background variability. (C)
687 Fold-change in the frequency of next-generation sequencing reads for variant mutations
688 at each site on hFlex3a2_v2 VL after panning, relative to their frequency in the initial
689 library, shows that certain residues that cluster in and around the CDRs have a large

690 increase in read frequency. (D) The percent distribution of all variants for each site of the
691 CDRs after two rounds of panning against *S. flexneri* 3a shows that at some sites (I29,
692 S30, H34) a single variant, or at other sites (L33, A51, N90, S93) a handful of variants
693 were enriched for. (E) Specificity of mutational enrichment was determined. Each dot
694 represents the enrichment of a variant against *S. flexneri* 3a relative to *S. sonnei* at the
695 indicated residue after two rounds of panning. Positive numbers indicate variants that
696 were enriched against *S. flexneri* 3a relative to *S. sonnei*, zero indicates similar
697 enrichment against both bacterial species, and negative numbers indicate variants that
698 were enriched for against *S. sonnei* relative to *S. flexneri* 3a. Dotted line is 20 standard
699 deviations above the mean mutation enrichment in the input library.
700
701 **Fig 4: Binding analysis of hFlex3a2_v2 variants specifically enriched against *S.*
702 *flexneri* 3a and produced as huIgG1 chimeras** (A) Surface staining experiment
703 confirms that 50 nM of the parental mAb (red), single amino acid variants (green), and
704 combinatorial variants (blue) bind *S. flexneri* 3a ~100-fold higher than a non-binding
705 control mAb (black) as indicated by a median fluorescence intensity. Surface staining is
706 the average of three biological replicates. Error bars represent standard deviation. (B)
707 Binding curves from a titration ELISA against *S. flexneri* 3a OMVs (2.5 μg/mL) show
708 relative binding potencies of the parent mAb (red), single amino acid variants (green),
709 and combinatorial variants (blue). ELISA binding curves are the average of three
710 independent replicates each performed in duplicate (C) EC_{50} values calculated from the
711 ELISA in panel B show relative steady-state apparent affinities of hFlex3a2_v2 variants.
712 Black line indicates the median EC_{50}. (D) Binding of hFlex3a2_v2, H34A, S30G + L33N,
713 and a non-binding control as huIgG1s to purified *S. flexneri* 3a O-Ag was assessed by
714 BLI. This experiment is the average of two experiments performed with independently
715 purified batches of mAbs.
716
717 **Fig 5: Functional analysis of hFlex3a2_v2 variants against *S. flexneri* 3a.** (A) L-ABA
718 assay comparing the ability of hFlex3a2_v2 variants and a non-binding control to
719 coordinate complement-mediated bacteriolysis of *S. flexneri* 3a. L-ABA is the average of
720 three biological replicates each performed in duplicate. p-values were calculated on
721 $logIC_{50}$ values by repeated measure Anova with Dunnett's correction for multiple
722 comparisons. (B) OPA assay measures the percent of THP-1 cells that have
723 phagocytosed *S. flexneri* 3a that was opsonized with 30 nM of the indicated mAb. This
724 experiment is the result of five biological replicates each performed in duplicate, and p-
725 values were calculated by repeated measure ANOVA with Dunnett's correction for
726 multiple comparisons. Error bars represent standard deviation. (C) Invasion assay shows
727 the percent invasion of *S. flexneri* 3a incubated with 1μM of the indicated mAb normalized
728 to the invasion rate of *S. flexneri* 3a in PBS. This experiment is the result of four biological
729 replicates each performed in duplicate, and p-values were calculated by repeated
730 measure ANOVA with Dunnett's correction for multiple comparisons. Errors bars
731 represent standard error of the mean (S.E.M.). For all plots, p values < 0.5 are denoted
732 by a *.
733
734 **Fig 6: Binding and functional analysis of hFlex3a2_v2 variants against *S. flexneri*
735 3b.** (A) Schematic depicting the O-Ag structures of our panel of *S. flexneri* serotypes. (B)

736 Surface staining with 50 nM of hFlex3a2_v2 variants and a non-binding control mAb to a
737 panel of *S. flexneri* and *S. sonnei* serotypes. This experiment is the average of two
738 replicates. (C) Binding curves from a titration ELISA against *S. flexneri* 3b OMVs (2.5
739 μg/mL) show relative binding potency of the parent mAb (red), single amino acid variants
740 (green), and combinatorial variants (blue). ELISA binding curves are the average of two
741 replicates. (D) L-ABA assay comparing the ability of hFlex3a2_v2, L33N, and S30G +
742 L33N to coordinate complement-mediated bacteriolysis of *S. flexneri* 3b. L-ABA is the
743 average of four biological replicates each performed in duplicate. (E) OPA assay
744 measures the percent of THP-1 cells that have phagocytosed *S. flexneri* 3b that was
745 opsonized with 30 nM of the indicated mAb. This experiment is the result of five biological
746 replicates each performed in duplicate, and p-values were calculated by repeated
747 measure ANOVA with Dunnett's correction for multiple comparisons. Error bars represent
748 standard deviation. (F) Invasion assay shows the percent invasion of *S. flexneri* 3b
749 incubated with 1μM of the indicated mAb normalized to the invasion rate of *S. flexneri* 3b
750 in PBS. This experiment is the result of four biological replicates each performed in
751 duplicate. Error bars represent standard error of the mean (S.E.M.). for all plots, p values
752 < 0.5 are denoted by a *.
753
754 **Fig S1**: **Mutation enrichment in the VH library after panning.** (A) Fold-change in the
755 frequency of next-generation sequencing reads for variant mutations at each VH site of
756 hFlex3a2_v2 after two rounds of panning, relative to their frequency in the input library.
757 (B) log10 enrichment of variants in the VH library after two rounds of panning against *S.*
758 *flexneri* 3a and *S. sonnei*. Dotted line is 20 standard deviations above the mean mutation
759 enrichment in the input library and indicates a stringent threshold set to distinguish
760 bacteria-mediated enrichment from background variability.
761
762 **Fig S2: Distribution of next-generation sequencing reads across the VL library**
763 **variants after panning.** A heatmap showing the percentage of all reads belonging to the
764 indicated hFlex3a2_v2 variant after two rounds of panning against *S. flexneri* 3a.
765
766 **Fig S3: Enrichment of VL mutations for increased affinity to the surface of *S.***
767 ***flexneri 3a* after two rounds of panning**. Enrichment of the indicated amino acids in the
768 library variants after panning against *S. flexneri* 3a was calculated relative to the
769 enrichment against *S. sonnei*. All data is log10 transformed. White squares with an "X"
770 through them indicate variants for which no reads were detected in either the input or
771 output libraries, suggesting that these variants may not have been successfully
772 synthesized.
773
774 **Fig S4: hFlex3a2_v2 variant *S. flexneri* 3a OMV and polyreactiviy ELISAs** (A) The
775 same ELISA as Figure 4B is reproduced here, but with all variants labeled. (B) ELISA
776 measuring non-specific binding of hFlex3a2_v2 variants to 5 μg/mL of insulin, CHO-
777 SMPs, or ssDNA. A known poly-reactive mAb (4E10 targeting HIV-1) and a known non-
778 polyreactive mAb (Adalimumab) serve as positive and negative controls, respectively.
779 This experiment is the result of three replicates. (C) Gating strategy for quantifying OPA.
780 Cells are gated first by size, then by CD45+ Dead- populations. An unrelated, nonbinding
781 mAb negative control is used to determine the %CTV+ gate.

Fig S5: L-ABA analysis of hFlex3a2_v2 variants against *S. flexneri* 3a (A) L-ABA from Fig 5A is reproduced here, but with all variants labeled. (B) log10 IC_{50} from L-ABA and EC_{50} from ELISA are correlated. R^2 represents Pearson correlation coefficient.

Fig S6: hFlex3a2_v2 variant ELISA against *S. flexneri* 3b OMVs. (A) SDS-PAGE of crude LPS extract from *S. flexneri* 3a and *S. flexneri* 3a waaL::kan (O-Ag-) confirms that knocking out waaL eliminates O-Ag expression. Gel was stained with Pro-Q Emerald 3000. (B)The ELISA from Fig 6C is reproduced here, but with all variants labeled.

Acknowledgements

The hFlex3a2 mAb was generated by the laboratory of Dr. Moon Nahm at the University of Alabama Birmingham in collaboration with the Walter Reed Army Institute of Research (36). We thank collaborators from the Wisconsin National Primate Research Center, Jennifer Hayes, Dr. Faye Hartmann, and Dr. Eric Peterson, for sharing isolates WS-016 and WS-037. We thank Finora Franck for invaluable program management support, Dr. Jon Heinrichs and Dr. Tawanda Mandizvo for a critical reading of this manuscript, Katherine McKenney for assistance with 10X sequencing, and Mark Ochoa for assistance with cell culture. We also thank Dr. Stephen Baker and Dr. Timothy Scott for scientific advice and support, as well as providing the Shigella sonnei 53G lvp::kan strain. Finally, we would like to thank current and former members of the RESISTANT Research Steering Group (including Wellcome Trust Program Officers) for their invaluable support of this work, including Dr. Pete Gardner, Dr. Colleen Loynachan, Dr. Kate Mills, Dr. Nathalie Herze-Vourc'h, and Dr. Christiane Gerke. This work was supported by the Wellcome Trust RESISTANT grant.

Works Cited:

1. GBD 2021 Antimicrobial Resistance Collaborators. Global burden of bacterial antimicrobial resistance 1990-2021: a systematic analysis with forecasts to 2050. Lancet Lond Engl. 2024 Sept 28;404(10459):1199–226.

2. La Guidara C, Adamo R, Sala C, Micoli F. Vaccines and Monoclonal Antibodies as Alternative Strategies to Antibiotics to Fight Antimicrobial Resistance. Int J Mol Sci. 2024 May 17;25(10):5487.

3. Perrett KP, Nolan TM, McVernon J. A Licensed Combined Haemophilus influenzae Type b-Serogroups C and Y Meningococcal Conjugate Vaccine. Infect Dis Ther. 2013 June;2(1):1–13.

4. Ladhani SN. Two decades of experience with the Haemophilus influenzae serotype b conjugate vaccine in the United Kingdom. Clin Ther. 2012 Feb;34(2):385–99.

5. Hedari CP, Khinkarly RW, Dbaibo GS. Meningococcal serogroups A, C, W-135, and Y tetanus toxoid conjugate vaccine: a new conjugate vaccine against invasive meningococcal disease. Infect Drug Resist. 2014;7:85–99.

824 6. Grijalva CG, Nuorti JP, Arbogast PG, Martin SW, Edwards KM, Griffin MR. Decline in
825 pneumonia admissions after routine childhood immunisation with pneumococcal conjugate
826 vaccine in the USA: a time-series analysis. Lancet Lond Engl. 2007 Apr 7;369(9568):1179–
827 86.

828 7. Milligan R, Paul M, Richardson M, Neuberger A. Vaccines for preventing typhoid fever.
829 Cochrane Database Syst Rev. 2018 May 31;5(5):CD001261.

830 8. Baker S, Krishna A, Higham S, Naydenova P, O'Leary S, Scott JB, et al. Exploiting human
831 immune repertoire transgenic mice for protective monoclonal antibodies against
832 antimicrobial resistant Acinetobacter baumannii. Nat Commun. 2024 Sept 12;15(1):7979.

833 9. Aguiar-Alves F, Le HN, Tran VG, Gras E, Vu TTT, Dong OX, et al. Antivirulence
834 Bispecific Monoclonal Antibody-Mediated Protection against Pseudomonas aeruginosa
835 Ventilator-Associated Pneumonia in a Rabbit Model. Antimicrob Agents Chemother. 2022
836 Feb 15;66(2):e0202221.

837 10. Nielsen TB, Yan J, Slarve M, Lu P, Li R, Ruiz J, et al. Monoclonal Antibody Therapy
838 against Acinetobacter baumannii. Infect Immun. 2021 Sept 16;89(10):e0016221.

839 11. Nielsen TB, Yan J, Luna BM, Talyansky Y, Slarve M, Bonomo RA, et al. Monoclonal
840 Antibody Requires Immunomodulation for Efficacy Against Acinetobacter baumannii
841 Infection. J Infect Dis. 2021 Dec 15;224(12):2133–47.

842 12. Richards AF, Doering JE, Lozito SA, Varrone JJ, Willsey GG, Pauly M, et al. Inhibition of
843 invasive salmonella by orally administered IgA and IgG monoclonal antibodies. PLoS Negl
844 Trop Dis. 2020 Mar;14(3):e0007803.

845 13. Gulati S, Beurskens FJ, de Kreuk BJ, Roza M, Zheng B, DeOliveira RB, et al. Complement
846 alone drives efficacy of a chimeric antigonococcal monoclonal antibody. PLoS Biol. 2019
847 June;17(6):e3000323.

848 14. Kalfopoulou E, Laverde D, Miklic K, Romero-Saavedra F, Malic S, Carboni F, et al.
849 Development of Opsonic Mouse Monoclonal Antibodies against Multidrug-Resistant
850 Enterococci. Infect Immun. 2019 Sept;87(9):e00276-19.

851 15. Pennini ME, De Marco A, Pelletier M, Bonnell J, Cvitkovic R, Beltramello M, et al. Immune
852 stealth-driven O2 serotype prevalence and potential for therapeutic antibodies against
853 multidrug resistant Klebsiella pneumoniae. Nat Commun. 2017 Dec 8;8(1):1991.

854 16. Rollenske T, Szijarto V, Lukasiewicz J, Guachalla LM, Stojkovic K, Hartl K, et al. Cross-
855 specificity of protective human antibodies against Klebsiella pneumoniae LPS O-antigen.
856 Nat Immunol. 2018 June;19(6):617–24.

857 17. Parzych EM, Gulati S, Zheng B, Bah MA, Elliott STC, Chu JD, et al. Synthetic DNA
858 Delivery of an Optimized and Engineered Monoclonal Antibody Provides Rapid and
859 Prolonged Protection against Experimental Gonococcal Infection. mBio. 2021 Mar
860 16;12(2):e00242-21.

861 18. Que YA, Lazar H, Wolff M, François B, Laterre PF, Mercier E, et al. Assessment of
862 panobacumab as adjunctive immunotherapy for the treatment of nosocomial Pseudomonas
863 aeruginosa pneumonia. Eur J Clin Microbiol Infect Dis Off Publ Eur Soc Clin Microbiol.
864 2014 Oct;33(10):1861–7.

865 19. Chastre J, François B, Bourgeois M, Komnos A, Ferrer R, Rahav G, et al. Safety, efficacy,
866 and pharmacokinetics of gremubamab (MEDI3902), an anti-Pseudomonas aeruginosa
867 bispecific human monoclonal antibody, in P. aeruginosa-colonised, mechanically ventilated
868 intensive care unit patients: a randomised controlled trial. Crit Care Lond Engl. 2022 Nov
869 15;26(1):355.

870 20. Healthcare G. ATS 2025: promising results with gremubamab in bronchiectasis [Internet].
871 Clinical Trials Arena. 2025 [cited 2025 Sept 8]. Available from:
872 https://www.clinicaltrialsarena.com/analyst-comment/ats-2025-promising-results-
873 gremubamab-bronchiectasis/

874 21. Erridge C, Bennett-Guerrero E, Poxton IR. Structure and function of lipopolysaccharides.
875 Microbes Infect. 2002 July;4(8):837–51.

876 22. Formal SB, Oaks EV, Olsen RE, Wingfield-Eggleston M, Snoy PJ, Cogan JP. Effect of prior
877 infection with virulent Shigella flexneri 2a on the resistance of monkeys to subsequent
878 infection with Shigella sonnei. J Infect Dis. 1991 Sept;164(3):533–7.

879 23. Cohen D, Meron-Sudai S, Bialik A, Asato V, Goren S, Ariel-Cohen O, et al. Serum IgG
880 antibodies to Shigella lipopolysaccharide antigens - a correlate of protection against
881 shigellosis. Hum Vaccines Immunother. 2019;15(6):1401–8.

882 24. Kappler K, Hennet T. Emergence and significance of carbohydrate-specific antibodies.
883 Genes Immun. 2020 Aug;21(4):224–39.

884 25. Haji-Ghassemi O, Blackler RJ, Martin Young N, Evans SV. Antibody recognition of
885 carbohydrate epitopes. Glycobiology. 2015 Sept;25(9):920–52.

886 26. Borenstein-Katz A, Warszawski S, Amon R, Eilon M, Cohen-Dvashi H, Leviatan Ben-Arye
887 S, et al. Biomolecular Recognition of the Glycan Neoantigen CA19-9 by Distinct
888 Antibodies. J Mol Biol. 2021 July 23;433(15):167099.

889 27. Amon R, Rosenfeld R, Perlmutter S, Grant OC, Yehuda S, Borenstein-Katz A, et al. Directed
890 Evolution of Therapeutic Antibodies Targeting Glycosylation in Cancer. Cancers. 2020 Sept
891 30;12(10):2824.

892 28. Haji-Ghassemi O, Müller-Loennies S, Brooks CL, MacKenzie CR, Caveney N, Van
893 Petegem F, et al. Subtle Changes in the Combining Site of the Chlamydiaceae-Specific mAb
894 S25-23 Increase the Antibody-Carbohydrate Binding Affinity by an Order of Magnitude.
895 Biochemistry. 2019 Feb 12;58(6):714–26.

896 29. Hu J, Huang X, Ling CC, Bundle DR, Cheung NKV. Reducing epitope spread during
897 affinity maturation of an anti-ganglioside GD2 antibody. J Immunol Baltim Md 1950. 2009
898 Nov 1;183(9):5748–55.

899 30. Thomas R, Patenaude SI, MacKenzie CR, To R, Hirama T, Young NM, et al. Structure of an
900 anti-blood group A Fv and improvement of its binding affinity without loss of specificity. J
901 Biol Chem. 2002 Jan 18;277(3):2059–64.

902 31. Brorson K, Thompson C, Wei G, Krasnokutsky M, Stein KE. Mutational analysis of avidity
903 and fine specificity of anti-levan antibodies. J Immunol Baltim Md 1950. 1999 Dec
904 15;163(12):6694–701.

905 32. Deng SJ, MacKenzie CR, Sadowska J, Michniewicz J, Young NM, Bundle DR, et al.
906 Selection of antibody single-chain variable fragments with improved carbohydrate binding
907 by phage display. J Biol Chem. 1994 Apr 1;269(13):9533–8.

908 33. Brummell DA, Sharma VP, Anand NN, Bilous D, Dubuc G, Michniewicz J, et al. Probing
909 the combining site of an anti-carbohydrate antibody by saturation-mutagenesis: role of the
910 heavy-chain CDR3 residues. Biochemistry. 1993 Feb 2;32(4):1180–7.

911 34. Yelton DE, Rosok MJ, Cruz G, Cosand WL, Bajorath J, Hellström I, et al. Affinity
912 maturation of the BR96 anti-carcinoma antibody by codon-based mutagenesis. J Immunol
913 Baltim Md 1950. 1995 Aug 15;155(4):1994–2004.

914 35. Wang W, Bunyatov M, Moffat D, Lopez-Barbosa N, DeLisa MP. Engineering affinity-
915 matured variants of an anti-polysialic acid monoclonal antibody with superior cytotoxicity-
916 mediating potency. Cell Chem Biol. 2025 Aug 21;32(8):1042-1057.e6.

917 36. Deng SJ, MacKenzie CR, Hirama T, Brousseau R, Lowary TL, Young NM, et al. Basis for
918 selection of improved carbohydrate-binding single-chain antibodies from synthetic gene
919 libraries. Proc Natl Acad Sci U S A. 1995 May 23;92(11):4992–6.

920 37. Lin J, Smith MA, Benjamin WH, Kaminski RW, Wenzel H, Nahm MH. Monoclonal
921 Antibodies to Shigella Lipopolysaccharide Are Useful for Vaccine Production. Clin Vaccine
922 Immunol CVI. 2016 Aug;23(8):681–8.

923 38. Mancini F, Gasperini G, Rossi O, Aruta MG, Raso MM, Alfini R, et al. Dissecting the
924 contribution of O-Antigen and proteins to the immunogenicity of Shigella sonnei generalized
925 modules for membrane antigens (GMMA). Sci Rep. 2021 Jan 13;11(1):906.

926 39. Kang TH, Seong BL. Solubility, Stability, and Avidity of Recombinant Antibody Fragments
927 Expressed in Microorganisms. Front Microbiol. 2020;11:1927.

928 40. Maynard JA, Maassen CBM, Leppla SH, Brasky K, Patterson JL, Iverson BL, et al.
929 Protection against anthrax toxin by recombinant antibody fragments correlates with antigen
930 affinity. Nat Biotechnol. 2002 June;20(6):597–601.

931 41. Chowdhury PS, Vasmatzis G. Engineering scFvs for improved stability. Methods Mol Biol
932 Clifton NJ. 2003;207:237–54.

933 42. Berry SK, Rust S, Caceres C, Irving L, Bartholdson Scott J, Tabor DE, et al. Phenotypic
934 whole-cell screening identifies a protective carbohydrate epitope on Klebsiella pneumoniae.
935 mAbs. 2022;14(1):2006123.

936 43. Perepelov AV, Shekht ME, Liu B, Shevelev SD, Ledov VA, Senchenkova SN, et al. Shigella
937 flexneri O-antigens revisited: final elucidation of the O-acetylation profiles and a survey of
938 the O-antigen structure diversity. FEMS Immunol Med Microbiol. 2012 Nov;66(2):201–10.

939 44. Doepker LE, Danon S, Harkins E, Ralph DK, Yaffe Z, Garrett ME, et al. Development of
940 antibody-dependent cell cytotoxicity function in HIV-1 antibodies. eLife. 2021 Jan
941 11;10:e63444.

942 45. Swindells MB, Porter CT, Couch M, Hurst J, Abhinandan KR, Nielsen JH, et al. abYsis:
943 Integrated Antibody Sequence and Structure-Management, Analysis, and Prediction. J Mol
944 Biol. 2017 Feb 3;429(3):356–64.

945 46. Brochet X, Lefranc MP, Giudicelli V. IMGT/V-QUEST: the highly customized and
946 integrated system for IG and TR standardized V-J and V-D-J sequence analysis. Nucleic
947 Acids Res. 2008 July 1;36(Web Server issue):W503-508.

948 47. Ye J, Ma N, Madden TL, Ostell JM. IgBLAST: an immunoglobulin variable domain
949 sequence analysis tool. Nucleic Acids Res. 2013 July;41(Web Server issue):W34-40.

950 48. Berlanda Scorza F, Colucci AM, Maggiore L, Sanzone S, Rossi O, Ferlenghi I, et al. High
951 yield production process for Shigella outer membrane particles. PloS One.
952 2012;7(6):e35616.

953 49. Han W, Wu B, Li L, Zhao G, Woodward R, Pettit N, et al. Defining function of
954 lipopolysaccharide O-antigen ligase WaaL using chemoenzymatically synthesized substrates.
955 J Biol Chem. 2012 Feb 17;287(8):5357–65.

956 50. Herring CD, Glasner JD, Blattner FR. Gene replacement without selection: regulated
957 suppression of amber mutations in Escherichia coli. Gene. 2003 June 5;311:153–63.

958 51. Heckman KL, Pease LR. Gene splicing and mutagenesis by PCR-driven overlap extension.
959 Nat Protoc. 2007;2(4):924–32.

960 52. Andris-Widhopf J, Rader C, Steinberger P, Fuller R, Barbas CF. Methods for the generation
961 of chicken monoclonal antibody fragments by phage display. J Immunol Methods. 2000 Aug
962 28;242(1–2):159–81.

963 53. Silva RP, DiVenere AM, Amengor D, Maynard JA. Antibodies binding diverse pertactin
964 epitopes protect mice from Bordetella pertussis infection. J Biol Chem. 2022
965 Mar;298(3):101715.

966 54. Cai H, Yao H, Li T, Hutter CAJ, Li Y, Tang Y, et al. An improved fluorescent tag and its
967 nanobodies for membrane protein expression, stability assay, and purification. Commun
968 Biol. 2020 Dec 10;3(1):753.

969 55. Micoli F, Rondini S, Gavini M, Pisoni I, Lanzilao L, Colucci AM, et al. A scalable method
970 for O-antigen purification applied to various Salmonella serovars. Anal Biochem. 2013 Mar
971 1;434(1):136–45.

972 56. Caradonna V, Pinto M, Alfini R, Giannelli C, Iturriza M, Micoli F, et al. High-Throughput
973 Luminescence-Based Serum Bactericidal Assay Optimization and Characterization to Assess
974 Human Sera Functionality Against Multiple Shigella flexneri Serotypes. Int J Mol Sci. 2024
975 Oct 16;25(20):11123.

976 57. Weinblatt ME, Keystone EC, Furst DE, Moreland LW, Weisman MH, Birbara CA, et al.
977 Adalimumab, a fully human anti-tumor necrosis factor alpha monoclonal antibody, for the
978 treatment of rheumatoid arthritis in patients taking concomitant methotrexate: the ARMADA
979 trial. Arthritis Rheum. 2003 Jan;48(1):35–45.

980 58. Elsinghorst EA. Measurement of invasion by gentamicin resistance. Methods Enzymol.
981 1994;236:405–20.

982 59. Darveau RP, Hancock RE. Procedure for isolation of bacterial lipopolysaccharides from both
983 smooth and rough Pseudomonas aeruginosa and Salmonella typhimurium strains. J Bacteriol.
984 1983 Aug;155(2):831–8.

985

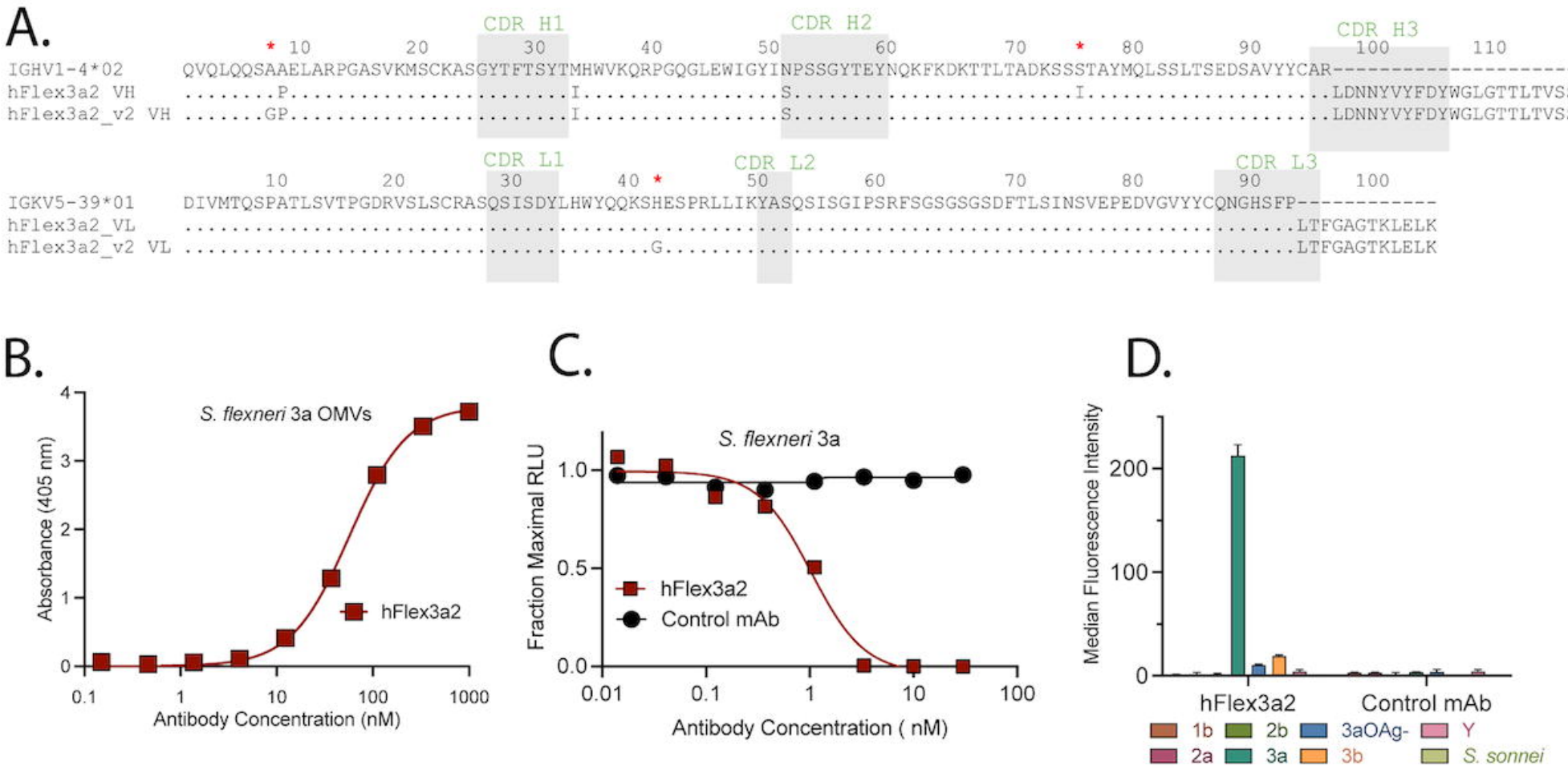
A.
CDR H1
CDR H2
CDR H3
* 10 20 30 40 50 60 70 * 80 90 100 110
IGHV1-4*02 QVQLQQSAAELARPGASVKMSCKASGYTFTSYTMHWVKQRPGQGLEWIGYINPSSGYTEYNQKFKDKTTLTADKSSSTAYMQLSSLTSEDSAVYYCAR----------
hFlex3a2 VH .....P.....I.....S.....I.....LDNNYVYFDYWGLGTTLTVSS
hFlex3a2_v2 VH .....GP.....I.....S.....LDNNYVYFDYWGLGTTLTVSS
CDR L1
CDR L2
CDR L3
10 20 30 40 * 50 60 70 80 90 100
IGKV5-39*01 DIVMTQSPATLSVTPGDRVSLSCRASQSISDYLHWYQQKSHESPRLLIKYASQSISGIPSRFSGSGSGSDFTLSINSVEPEDVGVYYCQNGHSFP----------
hFlex3a2_VL .....LTFGAGTKLELK
hFlex3a2_v2 VL .....G.....LTFGAGTKLELK
B.
S. flexneri 3a OMVs
Absorbance (405 nm)
hFlex3a2
Antibody Concentration (nM)
C.
S. flexneri 3a
Fraction Maximal RLU
hFlex3a2
Control mAb
Antibody Concentration (nM)
D.
Median Fluorescence Intensity
hFlex3a2
Control mAb
1b
2b
3aOAg-
Y
2a
3a
3b
S. sonnei

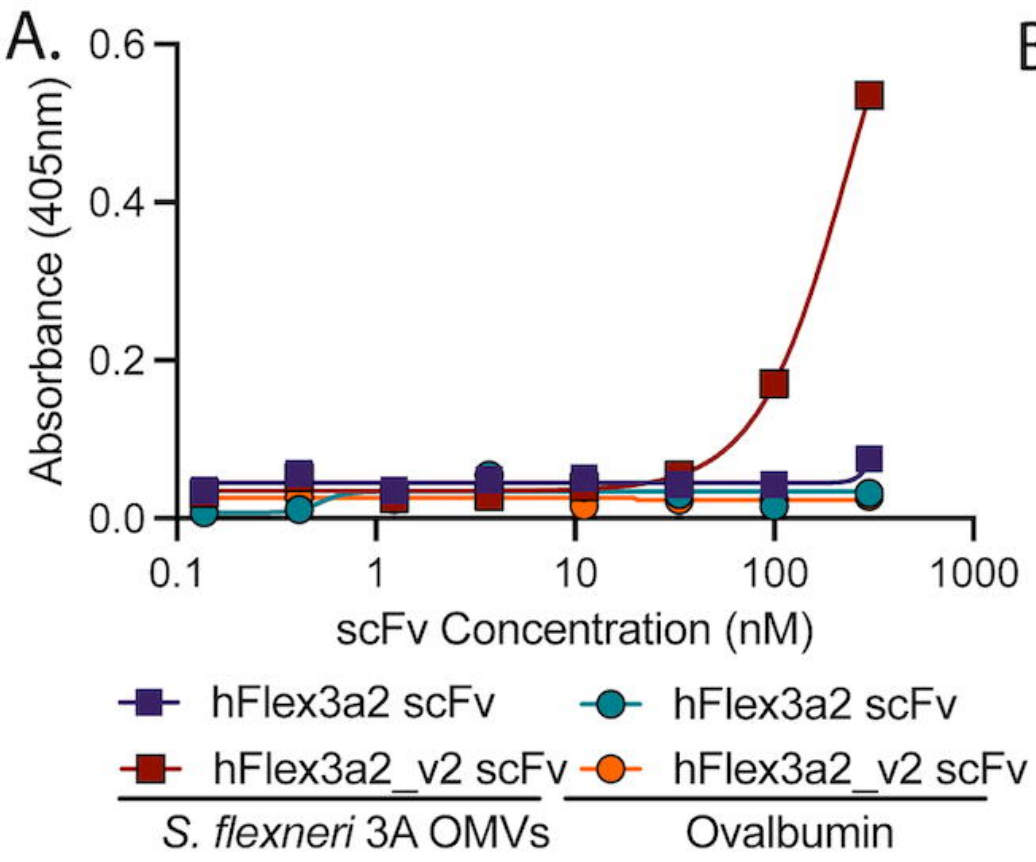
A.
Absorbance (405nm)
0.6
0.4
0.2
0.0
0.1
1
10
100
1000
scFv Concentration (nM)
hFlex3a2 scFv
hFlex3a2_v2 scFv
hFlex3a2 scFv
hFlex3a2_v2 scFv
S. flexneri 3A OMVs
Ovalbumin

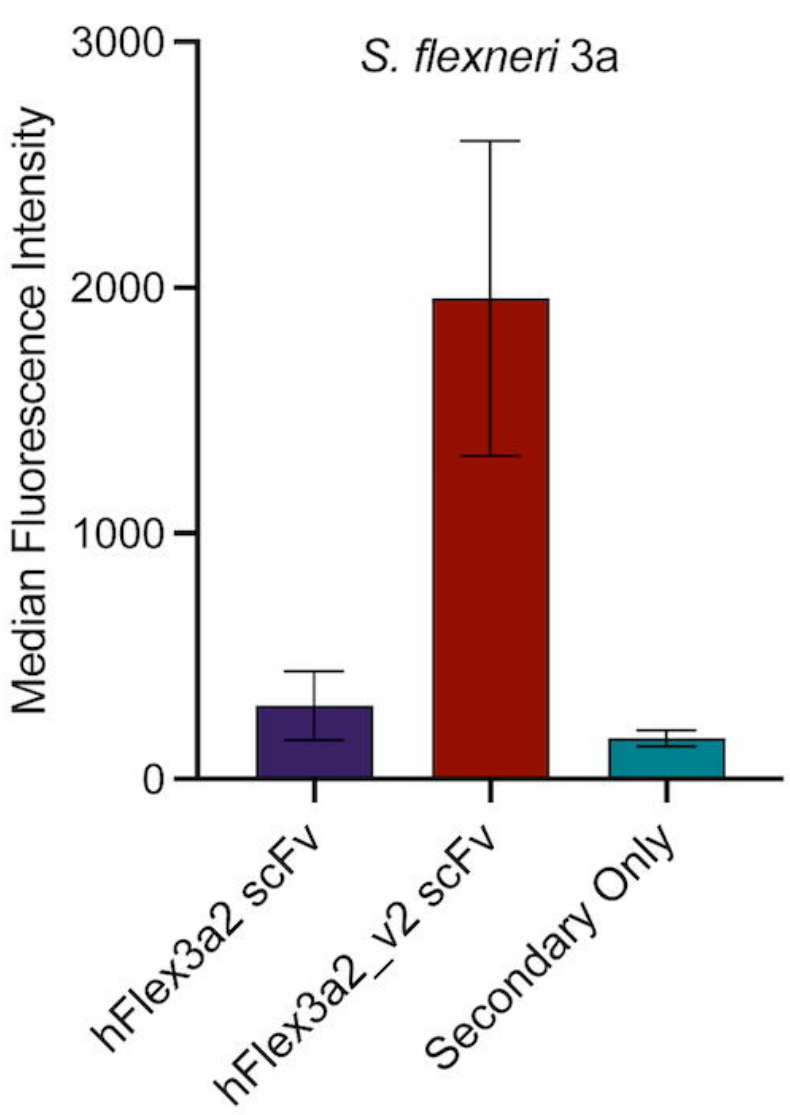
B.
S. flexneri 3a
Median Fluorescence Intensity
3000
2000
1000
0
hFlex3a2 scFv
hFlex3a2_v2 scFv
Secondary Only

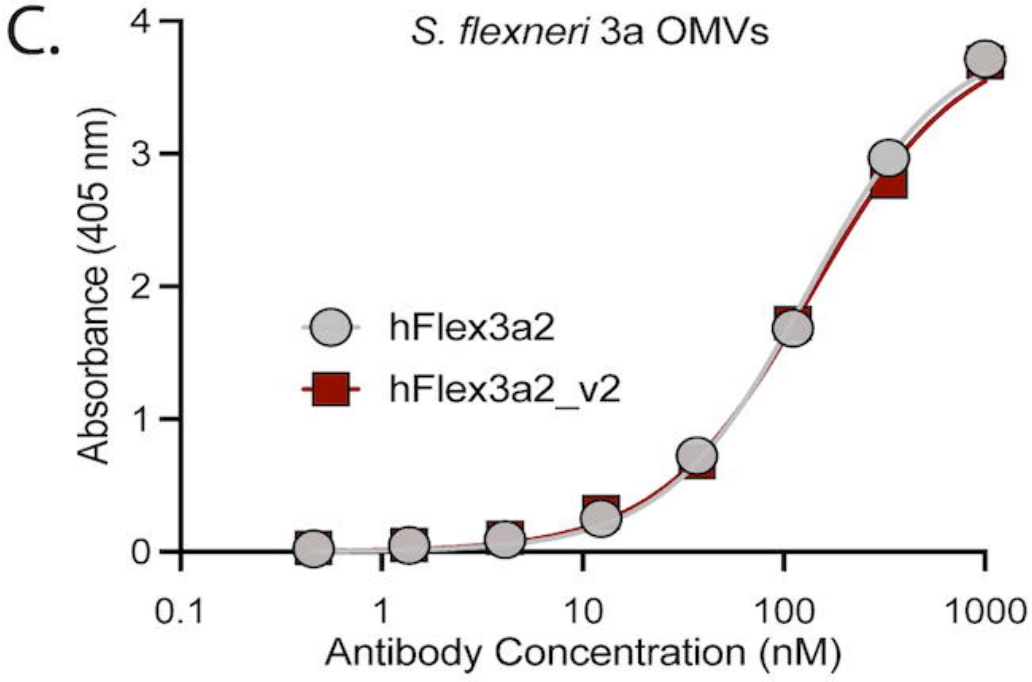
C.
S. flexneri 3a OMVs
Absorbance (405 nm)
4
3
2
1
0
hFlex3a2
hFlex3a2_v2
0.1
1
10
100
1000
Antibody Concentration (nM)

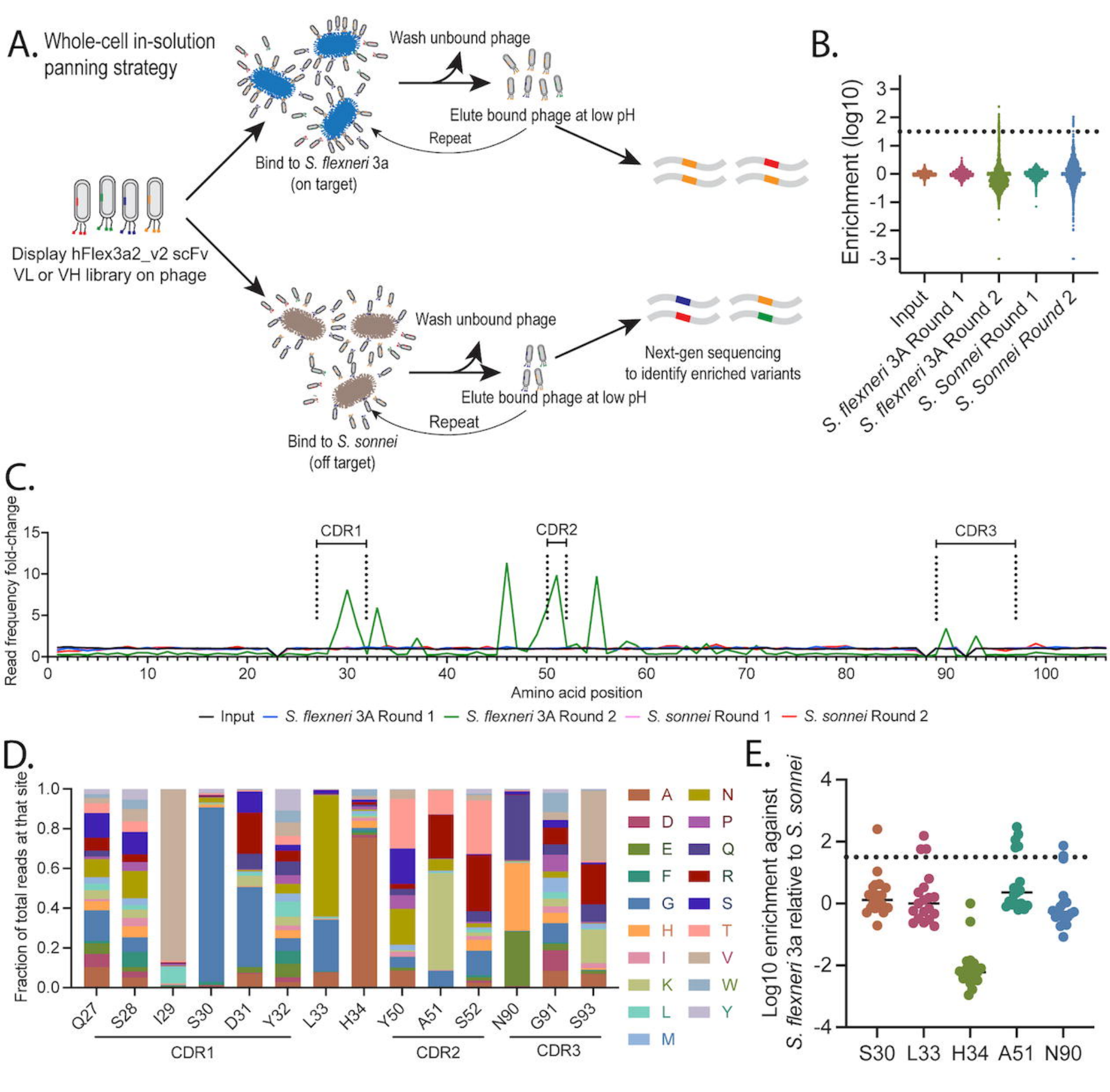
A.
Whole-cell in-solution panning strategy
Wash unbound phage
Elute bound phage at low pH
Repeat
Bind to S. flexneri 3a (on target)
Display hFlex3a2_v2 scFv VL or VH library on phage
Wash unbound phage
Elute bound phage at low pH
Repeat
Bind to S. sonnei (off target)
Next-gen sequencing to identify enriched variants
B.
Enrichment (log10)
Input
S. flexneri 3A Round 1
S. flexneri 3A Round 2
S. Sonnei Round 1
S. Sonnei Round 2
C.
Read frequency fold-change
CDR1
CDR2
CDR3
Amino acid position
Input
S. flexneri 3A Round 1
S. flexneri 3A Round 2
S. sonnei Round 1
S. sonnei Round 2
D.
Fraction of total reads at that site
Q27
S28
I29
S30
D31
Y32
L33
H34
Y50
A51
S52
N90
G91
S93
CDR1
CDR2
CDR3
A
D
E
F
G
H
I
K
L
M
N
P
Q
R
S
T
V
W
Y
E.
Log10 enrichment against S. flexneri 3a relative to S. sonnei
S30
L33
H34
A51
N90

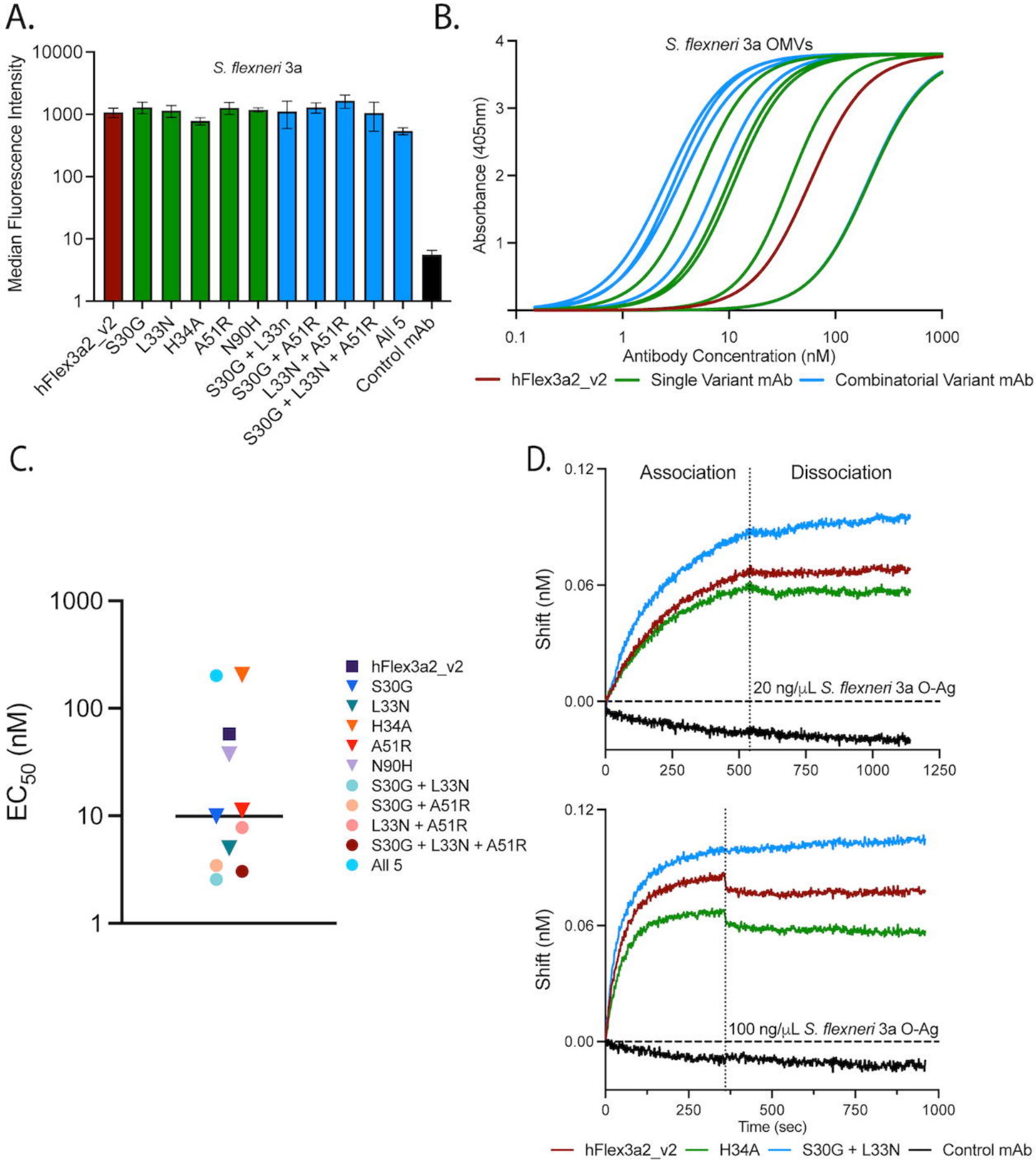
A.
S. flexneri 3a
Median Fluorescence Intensity
10000
1000
100
10
1
hFlex3a2_v2
S30G
L33N
H34A
A51R
N90H
S30G + L33n
S30G + A51R
L33N + A51R
S30G + L33N + A51R
All 5
Control mAb
B.
S. flexneri 3a OMVs
Absorbance (405nm)
Antibody Concentration (nM)
hFlex3a2_v2
Single Variant mAb
Combinatorial Variant mAb
C.
EC50 (nM)
hFlex3a2_v2
S30G
L33N
H34A
A51R
N90H
S30G + L33N
S30G + A51R
L33N + A51R
S30G + L33N + A51R
All 5
D.
Association
Dissociation
Shift (nM)
20 ng/μL S. flexneri 3a O-Ag
100 ng/μL S. flexneri 3a O-Ag
Time (sec)
hFlex3a2_v2
H34A
S30G + L33N
Control mAb

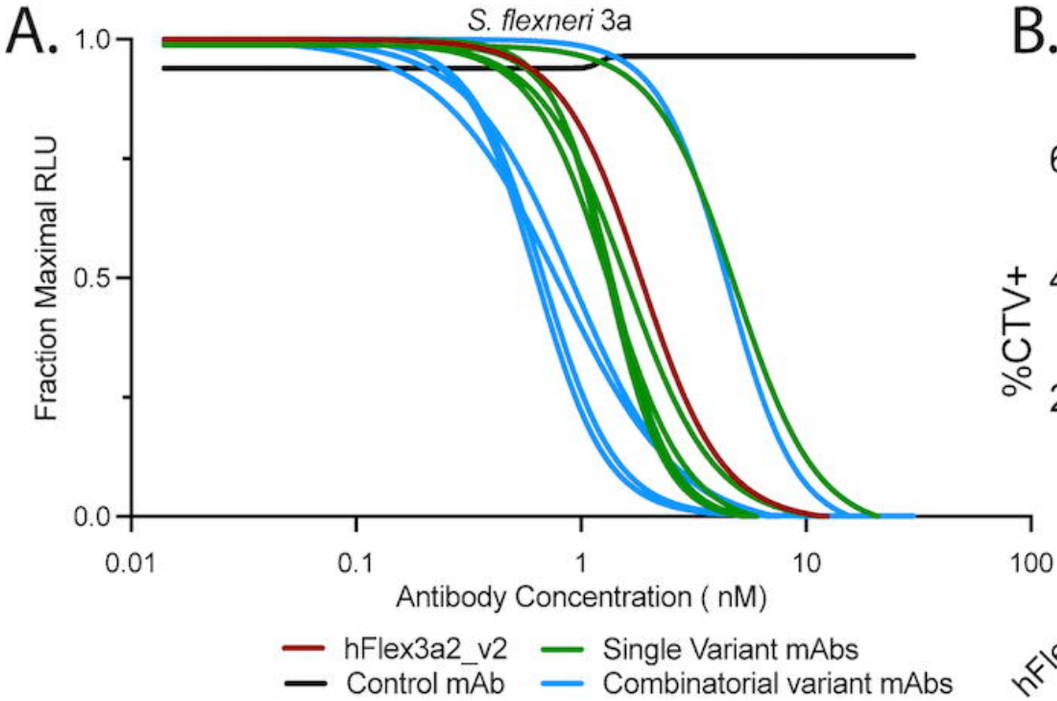
A.
S. flexneri 3a
Fraction Maximal RLU
1.0
0.5
0.0
0.01
0.1
1
10
100
Antibody Concentration (nM)
hFlex3a2_v2
Control mAb
Single Variant mAbs
Combinatorial variant mAbs

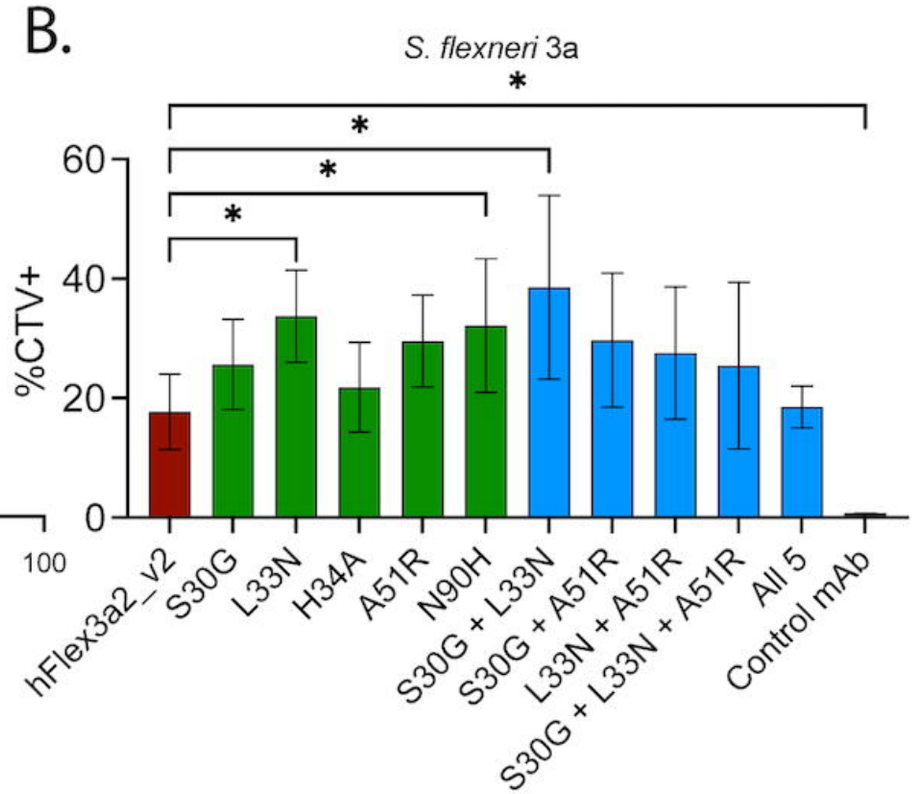
B.
S. flexneri 3a
%CTV+
60
40
20
0
*
hFlex3a2_v2
S30G
L33N
H34A
A51R
N90H
S30G + L33N
S30G + A51R
L33N + A51R
S30G + L33N + A51R
All 5
Control mAb

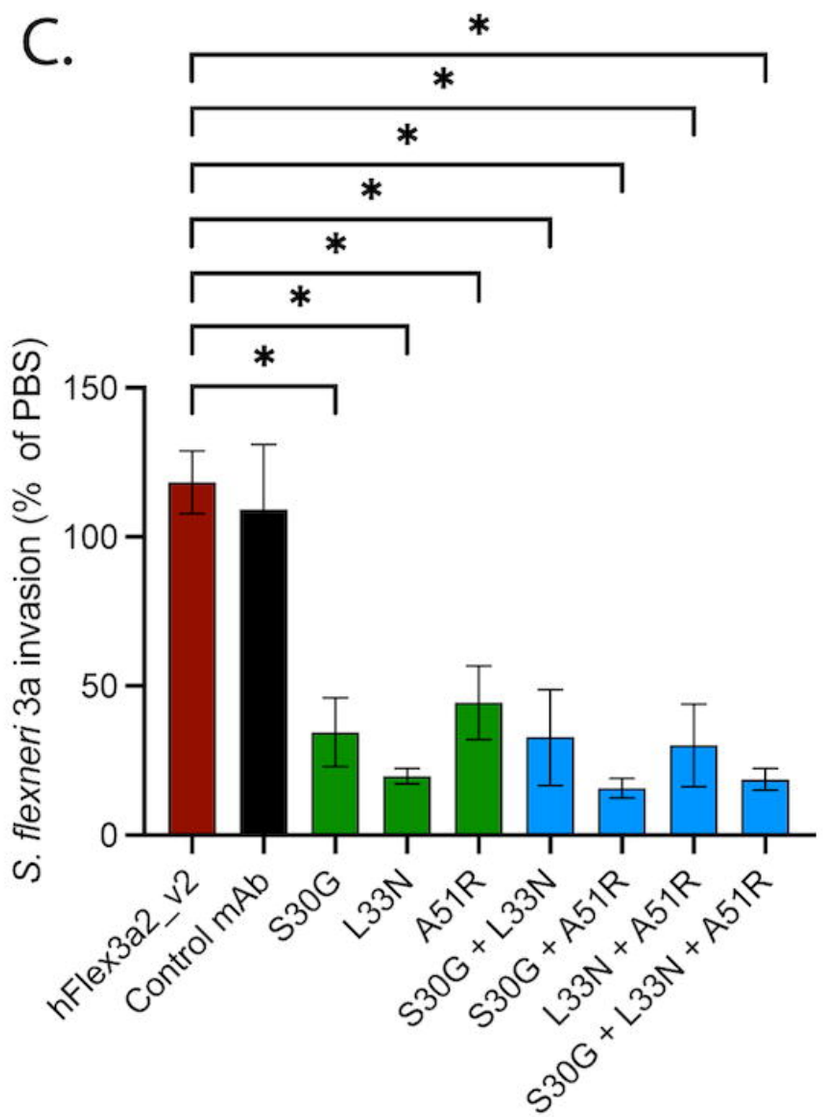
C.
S. flexneri 3a invasion (% of PBS)
150
100
50
0
*
hFlex3a2_v2
Control mAb
S30G
L33N
A51R
S30G + L33N
S30G + A51R
L33N + A51R
S30G + L33N + A51R

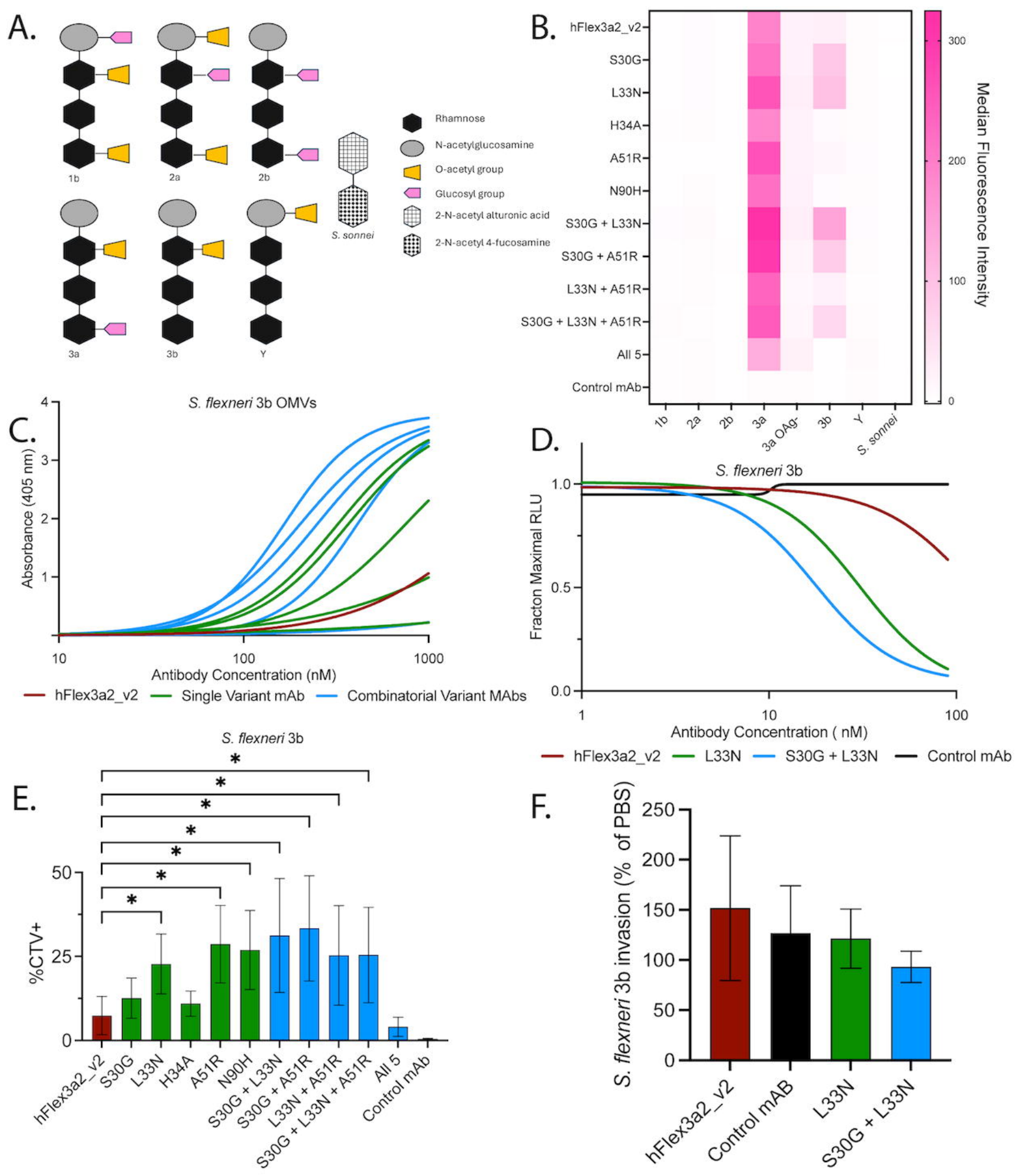
A.
1b
2a
2b
3a
3b
Y
S. sonnei
Rhamnose
N-acetylglucosamine
O-acetyl group
Glucosyl group
2-N-acetyl alturonic acid
2-N-acetyl 4-fucosamine
B.
hFlex3a2_v2
S30G
L33N
H34A
A51R
N90H
S30G + L33N
S30G + A51R
L33N + A51R
S30G + L33N + A51R
All 5
Control mAb
1b
2a
2b
3a
3a OAg-
3b
Y
S. sonnei
Median Fluorescence Intensity
300
200
100
0
C.
S. flexneri 3b OMVs
Absorbance (405 nm)
4
3
2
1
10
100
1000
Antibody Concentration (nM)
hFlex3a2_v2
Single Variant mAb
Combinatorial Variant MAbs
D.
S. flexneri 3b
Fracton Maximal RLU
1.0
0.5
0.0
1
10
100
Antibody Concentration (nM)
hFlex3a2_v2
L33N
S30G + L33N
Control mAb
E.
S. flexneri 3b
%CTV+
50
25
0
hFlex3a2_v2
S30G
L33N
H34A
A51R
N90H
S30G + L33N
S30G + A51R
L33N + A51R
S30G + L33N + A51R
All 5
Control mAb
F.
S. flexneri 3b invasion (% of PBS)
250
200
150
100
50
0
hFlex3a2_v2
Control mAB
L33N
S30G + L33N